Pulmonary Mechanics by Spectral Analysis of Forced Random Noise

EDWARD D. MICHAELSON, ERIC D. GRASSMAN, and WENDELL R. PETERS

From the Biodynamics Branch, Environmental Sciences Division, United States Air Force School of Aerospace Medicine, Aerospace Medical Division, Air Force Systems Command, Brooks Air Force Base, Texas 78235

ABSTRACT The magnitude ($|Z_{rs}|$) and phase angle (θ_{rs}) of the total respiratory impedance (Z_{rs}), from 3 to 45 Hz, were rapidly obtained by a modification of the forced oscillation method, in which a random noise pressure wave is imposed on the respiratory system at the mouth and compared to the induced random flow using Fourier and spectral analysis. No significant amplitude or phase errors were introduced by the instrumentation. 10 normals, 5 smokers, and 5 patients with chronic obstructive lung disease (COPD) were studied. Measurements of Z_{rs} were corrected for the parallel shunt impedance of the mouth, which was independently measured during a Valsalva maneuver, and from which the mechanical properties of the mouth were derived. There were small differences in Z_{rs} between normals and smokers but both behaved approximately like a second-order system with $\theta_{rs} = 0°$ in the range of 5–9 Hz, and θ_{rs} in the range of $+40°$ at 20 Hz and $+60°$ at 40 Hz. In COPD, θ_{rs} remained more negative (compared to normals and smokers) at all frequencies and crossed 0 between 15 and 29 Hz. Changes in Z_{rs}, similar to those in COPD, were also observed at low lung volumes in normals. These changes, the effects of a bronchodilator in COPD, and deviations of Z_{rs} from second-order behavior in normals, can best be explained by a two-compartment parallel model, in which time-constant discrepancies between the lung parenchyma and compliant airways keep compliant greater than inertial reactance, resulting in a more negative phase angle as frequency is increased.

INTRODUCTION

The description of the respiratory system in terms of electrical analogs (1) by Otis et al. (2) and others (3–15), has facilitated solutions to many problems involving the dynamic behavior of the lungs and chest. Most authors, as a first approximation, have considered the resistive, inertial, and elastic properties of the respiratory system analogous to a simple series resistance-inductance-capacitance (RLC)[1] electrical network or to a resistance-mass-spring mechanical system (3, 4, 9, 10 13).

There are numerous schemes for studying the properties of physical systems (17), although few have been applied to biological systems. DuBois et al. (3) first employed forced sinusoidal pressure oscillations at the mouth or around the thorax and measured the induced flow at the subject's mouth. By comparing the induced pressure and flow oscillations for magnitude and phase, he could determine the magnitude ($|Z_{rs}|$) and phase angle (θ_{rs}) of the impedance[2] for the total respiratory system at different frequencies (3–10 Hz) and confirm that it behaved approximately like a second-order system. At low frequencies, $|Z_{rs}|$ was high and θ_{rs} was negative (pressure-lagged flow) due to the elasticity or compliance of the system. As the frequency of induced oscillations increased, $|Z_{rs}|$ decreased and reached a minimum at about 6 Hz, the resonant frequency (f_n), at which θ_{rs} was 0 and $|Z_{rs}|$ was entirely resistive. As frequency was further increased, $|Z_{rs}|$ increased and θ_{rs} became positive (pressure-led flow) due to the inertial properties of the system. Many investigators have employed DuBois' technique or a modification to study respiratory mechanics in man and animals (4, 5, 7–10, 13, 18–25). With few exceptions (7, 8, 13), most observations are over a limited frequency range (3–10 Hz) and, in general, similar to those of DuBois et al. (3).

Dr. Michaelson's present address is the Division of Pulmonary Diseases, Mount Sinai Medical Center, Miami Beach, Fla. 33140.

Received for publication 31 July 1974 and in revised form 30 June 1975.

[1] The abbreviations used in this manuscript to describe the analogous properties of electrical, mechanical, and physiological systems will be as in reference 16 unless otherwise specified.

[2] The complex quantity impedance (Z) which has both real (resistive) and imaginary (reactive) parts can alternately be expressed in polar coordinates in terms of magnitude ($|Z|$) and phase (θ).

There have been few observations of respiratory impedance in man at frequencies greater than 10 Hz (7, 8, 13) and little data exist for θ_{rs} at frequencies other than resonance (3, 13). Virtually no information is available on $|Z_{rs}|$ and θ_{rs} at different frequencies in patients with lung disease, although respiratory resistance has been measured at multiple frequencies (10).

Our purpose was to develop a technique with which $|Z_{rs}|$ and θ_{rs} can be quickly and accurately obtained over an expanded frequency range with a frequency resolution impractical by conventional techniques. We have employed the technique in normal subjects and patients with obstructive pulmonary disease and interpreted the results in terms of electrical models of the lung. The hypothesis of Mead (11), that uneven time constants between the airways and parenchyma may be an important source of frequency-dependent compliance, has been evaluated and compared to other parallel two-compartment models.

The technique is a modification of the DuBois' method (3, 9, 25) except that a random noise pressure wave, containing all frequencies of interest, is imposed on the respiratory system and a random flow signal is induced. Until recently, analysis of wave forms other than sinusoidal has been a complex problem. However, with the development of various algorithms for efficient digital implementation of the fast Fourier transform (FFT) (26–28), it is now relatively easy to employ spectral analysis techniques (29–34) to determine the impedance of an unknown system. The Fourier transform (26–28) is a mathematical tool which can resolve any wave form into its individual frequency components. Thus, if a random pressure wave is imposed on the respiratory system, it can be resolved into a series of terms containing both magnitude and phase information which can be correlated with the resulting flow to obtain $|Z|$ and θ of the respiratory system at each frequency present in the input wave form. Similar techniques have been used by Taylor (35) to study aortic and femoral arterial impedance during random electrical pacing of the heart. Some advantages of spectral analysis techniques are speed of measurement and simultaneous determination of $|Z_{rs}|$ and θ_{rs} at each frequency of interest, reducing variability with frequency which may actually be due to time-dependent changes in the system.

METHODS

Principles of spectral analysis. With recent widespread use of computers, and the introduction of the FFT (26–28), digital solutions to cumbersome but powerful mathematical techniques for frequency analysis are now practical. The essential aspects of these techniques as they apply to this study will now be reviewed. For a more detailed consideration the interested reader is referred to references 26–34.

Fourier analysis is a mathematical tool for determining the frequency content of a time-varying signal. The Fourier transform (S_x) is the weighted integral of the time-varying function $x(t)$:

$$S_x = \int_{-\infty}^{\infty} x(t)e^{-j2\pi ft}dt = A_x + jB_x, \quad (1)$$

where f = frequency at which the integral is evaluated, t = time in seconds, and $j = \sqrt{-1}$. A_x and B_x are the real and imaginary components of S_x at frequency f, and contain magnitude and phase information of this frequency component of $x(t)$.

For a simple system with input $x(t)$ and output $y(t)$, the transfer function (H) can be obtained as follows:

$$H = \frac{S_y}{S_x} = \frac{\text{Fourier transform of output}}{\text{Fourier transform of input}}. \quad (2)$$

If $x(t)$ is random noise, H can be found at all frequencies in $x(t)$. If $x(t)$ is random pressure and $y(t)$ flow, then impedance is simply the reciprocal of H. Because of synchronization problems and statistical considerations related to the randomness of the input signal, the computation of H and Z by this method is not practical (32–34). Therefore, the concept of power spectra will be introduced. For the variables in the above system, S_x and S_y can be used to compute three power spectra. The input power spectrum is,

$$G_{xx} = S_xS_x^* = (A_x + jB_x)(A_x - jB_x) = A_x^2 + B_x^2, \quad (3)$$

where S_x^* is the complex conjugate of S_x. This product $(A_x^2 + B_x^2)$ no longer contains phase information. Similarly, the output power spectrum is,

$$G_{yy} = S_yS_y^* = A_y^2 + B_y^2. \quad (4)$$

The cross-power spectrum, defined as

$$G_{yx} = S_yS_x^* = (A_yA_x + B_yB_x) + j(B_yA_x - B_xA_y), \quad (5)$$

preserves the phase relationship between input and output signals and can be used to compute impedance, magnitude as follows:

$$|Z| = \frac{G_{xx}}{|G_{yx}|}. \quad (6)$$

The phase angle (θ) is contained in G_{yx} and is given by

$$\theta = -\tan^{-1}\frac{(B_yA_x - B_xA_y)}{(A_yA_x + B_yB_x)}. \quad (7)$$

The advantage of computing a transfer function or impedance in this way is the rapidity with which both phase and magnitude can be obtained over a wide range of frequencies. Further, the computation of Z does not depend on the character of $x(t)$, since Z is obtained as a ratio of the input and cross-power spectra. In other words, it is not required that $x(t)$ be gaussian white noise (33).

The principles outlined above apply to one input/one output, linear systems not contaminated by extraneous "noise." To apply spectral analysis in biological systems where these ideal conditions are unlikely, a method of

evaluating differences between input and output, which may be caused by factors other than the transfer characteristics of the system, is necessary. The coherence function (γ^2) provides this need.

$$\gamma^2 = \frac{|G_{yx}{}^2|}{G_{xx}G_{yy}} \quad 0 \leq \gamma^2 \leq 1. \tag{8}$$

γ^2 is a number between 0 and 1 similar to a correlation coefficient (33) and provides an index of causality between the input and output of a linear system. The value of γ^2 is less than 1 if the output is the result of more than one input, if the system is nonlinear, or if the system is contaminated by extraneous noise (e.g., electrical noise). Using γ^2, confidence limits for spectral estimates may be obtained (31, 33).

Data processing. To implement the Fourier transform (Eq. 1) on a digital computer, it is necessary to convert the continuous wave form into discrete samples. Because of this the frequency range over which reliable magnitude and phase information can be obtained is limited by the sample interval (Δt). Shannon's sampling theorem states that to define a sinusoid, slightly more than two equally spaced samples per period are required. This means that a time-varying wave form must be sampled at least twice the highest frequency of interest (F_{max}), that is

$$F_{max} < \frac{1}{2\Delta t}. \tag{9}$$

Once F_{max} or Δt are chosen, the basic frequency resolution or elementary bandwidth (Δf) and total record length or time of sample (T) are dictated by the size of the data array (N) available in the computer as follows:

$$T = N \times \Delta t \tag{10}$$

$$F_{max} = \frac{N}{2} \times \Delta f. \tag{11}$$

Actually, T or Δf could be chosen which would determine F_{max} and Δt. Limiting the value of T results in a finite number of data points and a truncated Fourier transform, the Discrete Finite transform (DFT) which can be digitally computed:

$$\text{DFT} = S_x' = \Delta t \sum_{n=0}^{N-1} x(n\Delta t)e^{-j2\pi(m\Delta f)\,n\Delta t}, \tag{12}$$

where $0 \leq m \leq N/2$, indicating that $N/2$ frequency components are produced by N samples of data.

In this study $F_{max} = 50$ Hz, hence pressure and flow were sampled at 100 Hz ($\Delta t = 0.01$ s). The data array size (N) was 64; therefore $T = 0.64$ s and $\Delta f = 1.5625$ Hz. A fully described point in the frequency domain must have both magnitude and phase represented by the real and imaginary parts of the DFT. Thus, when 0.64 s of data are sampled every 0.01 s resulting in 64 time points (N), a spectrum with $N/2 = 32$ frequency points, is computed; each point has two independent bits of information, magnitude and phase, at frequency intervals (Δf) of 1.5625 Hz. The power in Δf can be obtained from Eq. 3 and the resulting elementary spectral estimate is said to have 2 degrees of freedom, corresponding to a chi-square value of $\chi_2^2 = x_1^2 + x_2^2$ where x_1^2 and x_2^2 are analogous to A_x^2 and B_x^2 (Eq. 3). By averaging several (M) power spectra, confidence limits can be computed for the final spectral estimate about a chi-square distribution with $k = 2M$ degrees of freedom (31).

Ensemble averages of 25 spectra ($k = 50$) were computed requiring $25 \times 0.64 = 16$ s of pressure and flow data. Thus, at each frequency, the power spectra used to compute $|Z|$, θ, and γ^2 (Eqs. 3–8) represent an ensemble average of 25 frequency points. The relationships between γ^2, k, and the confidence intervals for magnitude and phase are given by the following equations (31). For the 100 $(1 - \alpha)$ percent confidence intervals:

$$|\bar{Z}| \left\{1 \pm \sqrt{\frac{2}{k-2} f_{2,k-2}(1-\alpha)\left(\frac{1-\gamma^2}{\gamma^2}\right)}\right\} \tag{13}$$

$$\bar{\theta} \pm \sin^{-1}\sqrt{\frac{2}{k-2} f_{2,k-2}(1-\alpha)\left(\frac{1-\gamma^2}{\gamma^2}\right)}, \tag{14}$$

where $|\bar{Z}|$ = ensemble average for $|Z|$, $\bar{\theta}$ = ensemble average for θ, k = equivalent number of degrees of freedom, and $f_{2,k-2}(1 - \alpha) = F$ distribution value corresponding to 2 and $k - 2$ degrees of freedom and cumulative probability $(1 - \alpha)$.

Two other factors are necessary to obtain reliable spectral estimates. The first is a phenomenon known as "aliasing" (29–34), wherein energy originating above F_{max} is "folded" back into the frequency range from 0 to F_{max}. This problem is remedied by sampling at a frequency slightly $>2F_{max}$ and by matched low-pass filtering of the input and output wave forms (see Hardware and Calibration), at a frequency slightly less than F_{max}, before sampling. The second factor, known as "leakage" (29–34), is a type of sampling error associated with the DFT. Leakage results from unsynchronized combinations of sampling rate (Δt) and length of data (T). This produces discontinuities at the beginning and end of the data sample (T) which can result in errors in the DFT. These leakage effects can be reduced by multiplying the sampled time data, before taking the DFT, by $|\frac{1}{2} - \frac{1}{2}\cos(2\pi t/T)|$, a bell-shaped function known as the Hanning window (29–34).[3]

The data reported in this study were processed on a Hewlett-Packard model 5451A Fourier analyzer (Hewlett-Packard Co., Palo Alto, Calif.) using a FFT subroutine based on the Cooley-Tukey algorithm (27) for implementing the DFT. The spectral analysis was written in assembly language and the statistical subroutines were written in FORTRAN. The results of a given measurement were immediately available on the oscilloscope screen of the Fourier analyzer and were stored on paper tape and printed on a teletype. Later, the results were plotted on a Hewlett-Packard model 7034A X-Y recorder. The results could be interchangebly displayed in polar coordinates as impedance magnitude and phase, or in rectangular coordinates as the real (resistance) and imaginary (reactance) parts of the impedance. The electrical impedance of a series RLC network determined both by sinusoidal and spectral analysis was virtually the same as the calculated values, providing an empirical check on the reliability of the analog hardware, the sampling techniques, and the computer program.

Hardware and calibrations. The apparatus is similar to that used in previous studies (10, 21, 23, 24) and is shown schematically in Fig. 1. Pressure fluctuations are induced

[3] In practice, this smoothing procedure may be implemented by convolving the Fourier transform of the time window with the Fourier transform of the input (pressure) and output (flow).

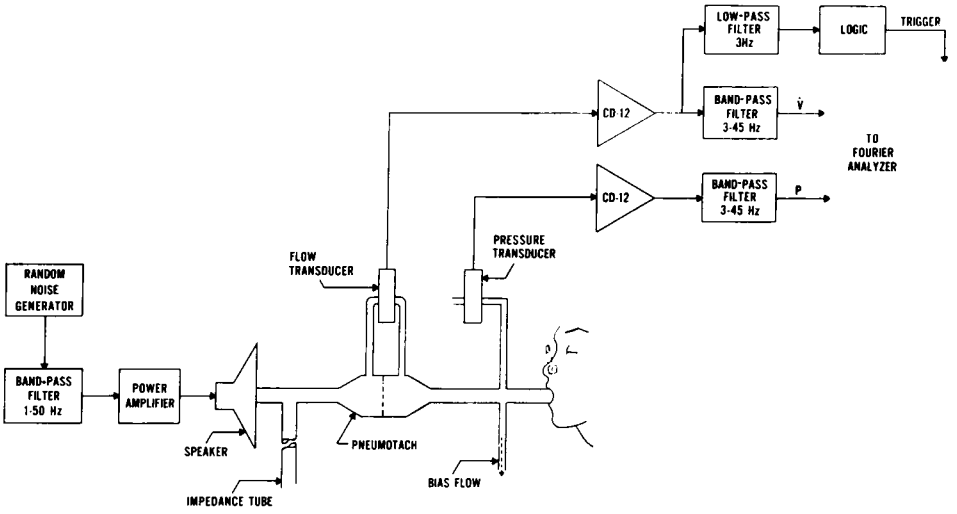

FIGURE 1 Schematic representation of the apparatus. Not shown are the subject's hands supporting his cheeks.

at the subject's mouth by a 12-inch loudspeaker (Acoustic Research, Inc., Cambridge, Mass.) and measured with a Validyne model DP45 (±2.5 cm H_2O) variable reluctance differential pressure transducer (Validyne Engineering Corp., Northridge, Calif.). The resulting flow was measured as the pressure drop, sensed with a matched Validyne DP45 transducer, across a Silverman (screen type) pneumotachograph (R = 0.2 cm H_2O/liter per s). The amplified pressure and flow signals (Validyne model CD-12 carrier demodulators) were band-pass filtered between 3 and 45 Hz (Krohn-Hite model 3343R, Krohn-Hite Corp., Cambridge, Mass.), thus eliminating both respiratory and high-frequency (to minimize aliasing) variations from the induced pressure and flow fluctuations. The pressure and flow signals were processed as already discussed. The flow signal was also low-pass filtered (3 Hz), and used to identify various parts of the respiratory cycle. A long, large bore tube (Fig. 1) provides a low impedance to the subject's low frequency respiration but, as an acoustical inductor, impedes the higher frequencies which are then induced at the subject's mouth. A continuous 0.5-liters/s bias flow eliminates CO_2 buildup.

The loudspeaker was driven with a random noise signal via a transistorized power amplifier (Hewlett-Packard model 6823A). The noise signal was produced with a Burr-Brown model 4006/25 noise generator function module (Burr-Brown Research Corp., Tucson, Ariz.). When a periodic clocking signal (square wave) is applied, this module generates random binary noise which, after low-pass or band-pass linear filtering, will produce a gaussian white, analog noise signal over a bandwidth which is small (1/4) compared to the clocking frequency. A 200-Hz square-wave clocking signal was used in this study and the binary output was band-pass filtered (1–50 Hz), resulting in analog random noise with a gaussian amplitude distribution. An example of the random pressure and flow signals that were used in this study is shown in Fig. 2.

The frequency response of the two pressure transducers, their associated Tygon tubing (0.476 cm ID × 10 cm long) (U. S. Stoneware Co., Akron, Ohio) and amplifiers was checked by response to a step input (36) and to a sinusoidal input, the latter by comparison to a catheter tip transducer (Millar model PC 350, Millar Instruments Inc., Houston, Tex.), shown (impulse response) to be flat ± <1% to 5 kHz. Both DP45 transducers were flat ±1% to 25 Hz and 1 dB up at 50 Hz. With both DP45 transducers measuring a common pressure (the opposite port of each referenced to

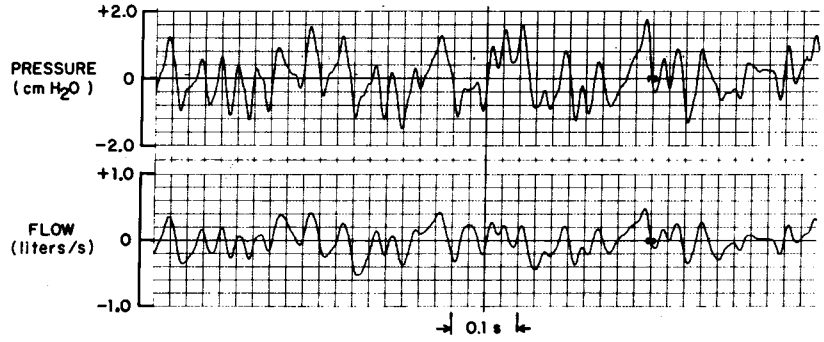

FIGURE 2 Example of induced random oscillations of pressure and flow.

atmosphere), there was less than 1° phase shift between, and less than 1% difference in, the amplitude ratio of the two transducers (and their respective amplifiers and filters) from 3 to 50 Hz.

The pneumotachograph was calibrated *in situ* with continuous flow from a rotameter. Although the pressure and flow transducers are matched for both amplitude and phase over the frequency range of interest, it is necessary to test the dynamic properties of the pneumotachograph to determine if any phase shift is introduced by the pneumotachograph itself. In this regard, the screen-type pneumotachograph should be better than the Fleisch, since the amount of gas that needs to be accelerated (and thus the inertance) is very small in the former, as confirmed by Finucane et al. (37) and Peslin et al. (38). The dynamic relationship between the pressure and flow measuring systems was tested by determination of the impedance and phase of a purely elastic system, the adiabatic compression of a mass of gas (38). This was accomplished by replacing the subject, on the apparatus shown in Fig. 1, with a large, wide-mouth bottle and comparing the induced random pressure and flow signals using spectral analysis. The phase angle between pressure and flow was $-90° \pm < 1°$ from 3 to 40 Hz, and $< \pm 3°$ at 45 Hz, indicating that the pneumotachograph (and associated electronics) provides reliable information as to the phase of flow over this frequency range.

Lung volumes and flow rates were measured with a water-filled spirometer. Functional residual capacity (FRC) and airway resistance (R_{aw}) were determined by body plethysmography (39).

Procedure. 10 normal subjects, 5 smokers, and 5 patients with chronic obstructive pulmonary disease (COPD) were studied in the sitting position while breathing quietly into the apparatus (Fig. 1) via a rubber mouthpiece. A noseclip was worn and the cheeks compressed with the palms. After 30 s of breathing, the subject performed an inspiratory vital capacity to standardize the volume history of the lung. After another 30–60 s of quiet breathing, 16 s of pressure and flow data were simultaneously sampled during continuous respiration, and processed on line as outlined above under Data Processing. For a given subject, the time required to obtain a phase or impedance plot on the oscilloscope screen of the Fourier analyzer was approximately 20 s. Additionally, by use of appropriate logic circuits, the low-pass (3 Hz) filtered flow signal was used to trigger the Fourier analyzer so that the induced pressure and flow signals were sampled and analyzed only at FRC, or during early inspiration when respiratory flow was between 0.25 and 0.50 liters/s. Although the data thus obtained represent different time samples of the respiratory system, it can be used for an approximate comparison of phase and impedance data between various portions of the respiratory cycle. One of the subjects with COPD (R. C.) was studied before and after inhalation of isoproteranol. In one normal subject (E. M.), impedance was measured during slow panting (1–1.5 Hz) at FRC and at different volumes, from 2 liters below to 2.5 liters above FRC. Also, in the same subject, impedance was measured, during quiet breathing, while simulated upper airway obstruction was produced by mild external tracheal compression.

The relationship between resistance and flow in the respiratory system is determined, in part, by turbulence related to the geometry of the airways. Thus, potential variation in the impedance could occur due to different flow rates. The magnitude of the induced oscillations was such that the effective magnitude of the induced random flow signal was equivalent to a sinusoidal flow of ± 0.32 liters/s $\pm < 10\%$ for the normal subjects and ± 0.28 liters/s $\pm < 20\%$ for the obstructed groups.[4]

In each subject, the impedance (Z_M') of the mouth (including oral cavity cheeks, pharynx, and larynx) and mouthpiece was determined by spectral analysis of the induced pressure and flow during a Valsalva maneuver[5] (cheeks compressed with palms). Since Z_M' is acoustically in parallel with the remainder of the respiratory system (Z_{rs}), this measurement can be used to correct the impedance measurements obtained during quiet breathing (Z_{rs}') for the characteristics of the mouth, to obtain the true Z_{rs} (peripheral to the glottis) as follows:

$$Z_{rs} = \frac{Z_M' \times Z_{rs}'}{Z_M' - Z_{rs}'}. \tag{15}$$

This computation was performed as a subroutine to the spectral analysis program. The measurement of Z_M' includes and corrects for the characteristics of the mouthpiece and the compressability of gas in the flowmeter-mouthpiece assembly. Additionally, an impedance measurement was made with the mouthpiece occluded and a correction, similar to Eq. 15, was applied to obtain the true impedance of the mouth (Z_M). In two subjects (E. M. and E. G.), Z_M was obtained with the cheeks unsupported and relaxed.

RESULTS

The spirometric data, FRC, and airway resistance are shown, along with the anthropometric data on each subject, in Table I.

The magnitude ($|Z_M'|$) and the phase angle (θ_M') of the mouth impedance (Z_M'), measured during a Valsalva maneuver, is shown for all the subjects in Fig. 3. Z_M' also includes the gas compressability and other mechanical properties of the mouthpiece assembly. The effects of Z_M' on the observed respiratory impedance (Z_{rs}') measured during continuous respiration, inspiration, or at FRC, were eliminated by applying Eq. 15 to obtain the true total respiratory impedance (Z_{rs}). The measured Z_{rs}' on each subject was individually corrected with his own Z_M'.

[4] The effective magnitude of oscillatory flow is determined by the average deviation of the flow magnitude from 0. Effective sinusoidal flow ($\dot{V}_s$) = $2/\pi \times$ the amplitude of the sine wave or $2\sqrt{2}/\pi \times$ its RMS (root mean square) value (RMS_s). Effective flow with a gaussian amplitude distribution ($\dot{V}_n$) = $\sqrt{2}/\pi \times$ its RMS value (RMS_n). Thus $RMS_n = 2/\sqrt{\pi} \times RMS_s$. $\dot{V}_n$ was measured with an absolute value circuit in series with a low-pass filter and the equivalent sinusoidal flow calculated as $\pm\pi/2 \times \dot{V}_n$. These relationships were verified by comparing the RMS and effective values of different magnitudes of random, sinusoidal, and steady flow by measuring the resistance of a small pneumotachograph.

[5] To eliminate the difficulty of performing a prolonged Valsalva maneuver (expiratory effort against a closed glottis), Z_M' was measured during five separate 10-s periods, during each of which 10 ensembles were obtained and the results from the five periods averaged ($M = 50$, $k = 100$ for the Z_M' measurement). This prolonged total patient time to approximately 3 min. Equivalent sinusoidal flow during measurement of $Z_M' = \pm 0.16$ liters/s.

TABLE I

Anthropometric, Spirometric and Plethysmographic Data

Group	Subject*	Age	Height	Weight	Vital capacity	FEV_1	FEV_3	MMEFR§‡	FRC	R_{aw}
		yr	*cm*	*kg*	*liters/BTPS‡*	*% vital capacity*		*liters/s*	*liters/BTPS‡*	*cm H_2O/liter/s*
Normal	H. E.	37	190.6	77.1	6.41	82.0	99.7	5.10	6.70	1.43
	J. R.	21	170.2	61.2	5.42	78.4	100.0	3.78	3.46	1.67
	D. H.	24	183.0	77.1	5.49	92.3	100.0	7.04	2.85	1.18
	E. G.	30	177.8	72.6	5.39	84.9	100.0	4.80	3.20	1.70
	D. E.	25	175.0	68.0	5.85	87.2	98.5	6.02	3.60	1.32
	S. S.	21	185.5	72.6	6.25	75.5	99.7	3.86	4.25	1.80
	R. O.	42	181.5	70.3	5.71	85.4	97.7	5.55	4.53	0.84
	R. D.	26	178.5	72.6	5.31	81.0	98.5	4.32	3.33	2.08
	T. G.	29	175.3	68.0	5.09	84.1	96.4	4.48	2.92	1.44
	E. M.	31	170.0	63.0	5.21	88.3	100.0	5.35	3.10	1.07
Smokers	A. M.	36	182.0	77.1	5.23	91.8	100.0	5.92	3.57	1.45
	T. C.	21	180.0	68.0	5.92	82.1	100.0	4.60	3.20	1.86
	J. J.	59	175.3	69.8	4.77	69.8	85.5	1.92	4.39	1.37
	S. H.	40	183.0	81.6	4.26	88.8	97.7	4.19	3.10	1.47
	J. N.	37	180.0	96.1	5.13	86.3	99.4	4.87	3.30	0.97
COPD	W. S.	42	177.7	86.2	3.99	64.2	83.9	1.23	3.00	2.52
	G. L.	51	175.3	68.7	2.72	41.0	67.8	0.33	5.69	6.71
	F. H.	50	178.4	68.0	4.47	52.7	79.6	1.02	5.58	2.33
	R. B.	39	188.0	72.1	4.88	52.3	77.7	1.01	5.40	2.89
	R. C.	55	177.7	70.3	3.21	49.4	78.2	0.33	5.96	3.28

* All males.

‡ BTPS, body temperature and pressure, saturated with water vapor.

§ Measured between 25 and 75% of VC.

An example of this correction, shown in Fig. 4, illustrates the effect of Z_M' on the phase angle and magnitude of the total respiratory impedance, in a normal subject (E. M.), during quiet breathing, with and without simulated upper airway obstruction, induced by external tracheal compression.

Since Z_M' is large compared to Z_{rs}' and the variability about Z_M' is small (95% confidence intervals [CI] $< \pm 5\%$), the error in Z_{rs} introduced by correcting Z_{rs}' for Z_M' is small and is less than the variability about Z_{rs}' estimates. Also, it makes little difference if Z_{rs}' on a given subject is corrected to Z_{rs} using the mean Z_M' of all the subjects or that individuals Z_M' ($< \pm 10\%$ for Z_{rs}, $< \pm 4°$ for θ_{rs}, and <1 Hz for f_n).

It is possible to obtain the true impedance of the mouth (Z_M) (Fig. 5) by applying a correction, similar to Eq. 15, to Z_M' using the impedance of the occluded mouthpiece assembly. Since the resonant frequency of the mouth is high (40 Hz), it is possible to estimate the value of compliance (C_M) from the reactance (X_M) at low frequencies (5 Hz) and inertance (I_M) is computed assuming that Z_M is second-order (Table II). The degree to which the latter assumption is true is illustrated in Fig. 5. Also shown in Fig. 5 is Z_M measured in two subjects with their cheeks unsupported and allowed to bulge during the forced oscillations. Compared to the supported cheeks, $|Z_M|$ is less at the lower frequencies, probably due to increased C_M (estimated as above to be 0.0028 liters/cm H_2O) of the unsupported cheeks and the shape of Z_M and θ_M vs. frequency is

TABLE II

*Mechanical Properties of the Mouth**

	C_M	I_M	f_n
	liters/cm $H_2O \times 10^{-4}$	*cm H_2O/liter/s^2*	*Hz*
Mean	10.09	0.0174	39.4
Min	5.79	0.0108	30.0
Max	18.72	0.0229	45.0
SD	3.09	0.0037	4.1

* Mean, range, and SD, in 19 subjects, of f_n and estimated compliance (C_M) and inertance (I_M) of the mouth (cheeks supported). These parameters were obtained individually, based on each individuals Z_M. Thus, the minimum and maximum values listed for C_M, I_M, and f_n do not coincide with a given subject, and f_n calculated from the mean estimated C_M and I_M is slightly less than the true mean f_n.

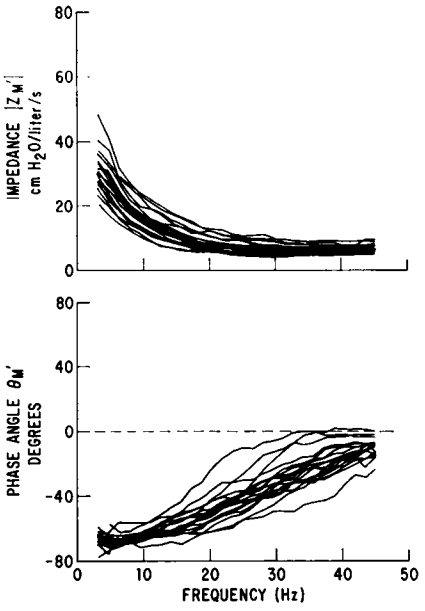

FIGURE 3 Magnitude and phase angle of the mouth impedance (including the mouthpiece assembly) for each subject. Each curve represents an average of 50 points at each of 32 frequencies, spaced 1.56 Hz.

more complex, indicating that Z_M is determined by higher order characteristics. R_M may be derived from the data in Fig. 5 as $|Z_M| \cos\theta_M$. The mean R_M (cheeks supported) was frequency dependent, falling from 11.4 (5.6 SD) cm H_2O/liter per s at 3 Hz to 7.3 (2.2 SD) at 30 Hz, and increasing to 8.0 (2.2 SD) at 40 Hz.

The data shown in Figs. 6–10 is corrected for mouth impedance and represents the respiratory system distal to the larynx. Fig. 6 shows, in two normal subjects, the type of magnitude and phase data obtained along with coherence (γ^2) and the 95% CIs (Eqs. 13 and 14). In general γ^2 tended to be slightly less and the CIs wider at the lower frequencies and during continuous respiration compared to the measurements made during inspiration only.

$|Z_{rs}|$ and θ_{rs}, measured during continuous respiration, are shown for nine normal subjects in Fig. 7. Each magnitude and phase curve in Figs. 4, 6, 7, 9, and 10 consists of an average of 25 complex points ($k = 50$) at each of 32 frequencies, spaced at $\Delta f = 1.56$ Hz.

The mean $|Z_{rs}|$ and θ_{rs} obtained during continuous respiration and during selective sampling of the respiratory cycle (FRC and inspiration), are shown in Fig. 8 for the normals, smokers, and subjects with COPD. Listed in Table III are individual values of $|Z_{rs}|$ and

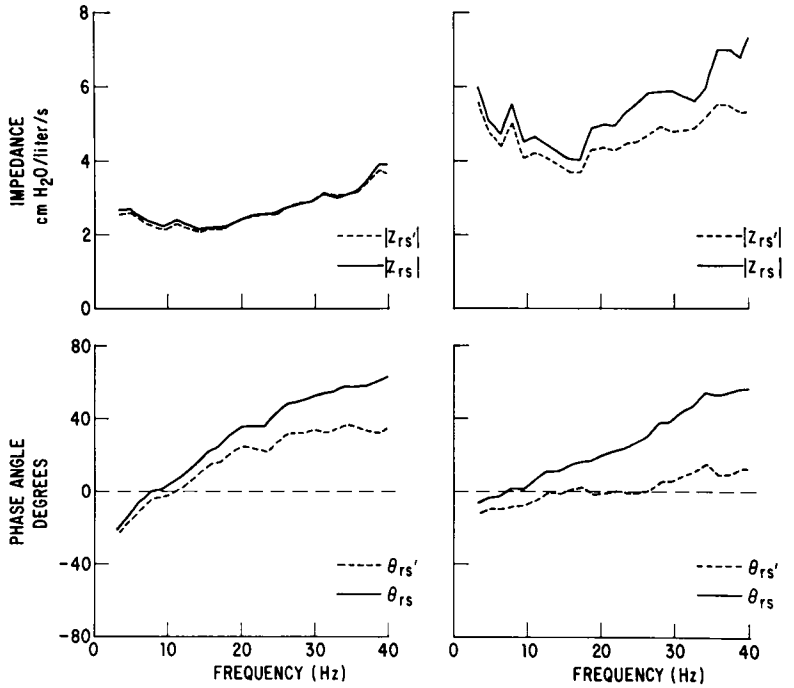

FIGURE 4 Effect of the parallel impedance of the mouth on the observed respiratory impedance (broken curves). Subject E. M. during quiet breathing without (left panels) and with (right panels) tracheal compression. The solid curves represent the corrected measurements (Eq. 15).

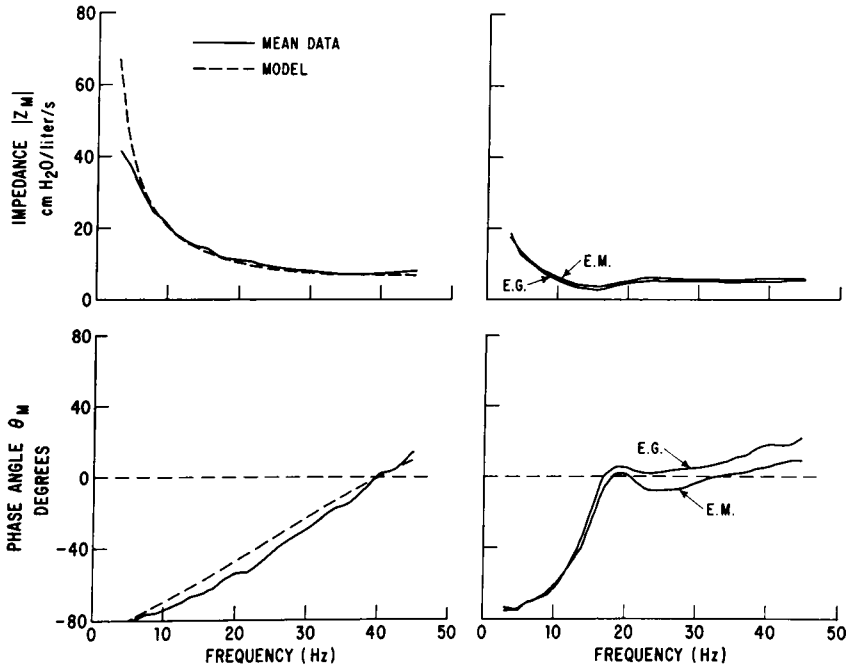

FIGURE 5 The solid curves in the left panels show the mean $|Z_M|$ and θ_M (corrected for mouthpiece assembly) for the 20 subjects with cheeks supported. The broken curves represent a second-order model, the coefficients of which were derived from the mean data. The right panels show $|Z_M|$ and θ_M in two subjects with the cheeks unsupported and allowed to bulge during the forced oscillations.

θ_{rs} at selected frequencies, illustrating the variability among normal subjects and those with varying degrees of obstruction, as well as differences between phases of the respiratory cycle.

The minimum value for $|Z_{rs}|$ occurred at a frequency somewhat higher than the resonant frequency (f_n), depending on the subject group and the phase of the respiratory cycle. For the data obtained at FRC the mean and range (in parenthesis) of the difference, between the frequency where $|Z_{rs}|$ was minimum and f_n, for the three groups of subjects are as follows: normals, 2.17 Hz (−0.20–9.50); smokers, 2.70 Hz (1.30–5.40); COPD, 5.60 Hz (1.80–8.00). The minimum values for $|Z_{rs}|$ were only slightly less than $|Z_{rs}|$ at f_n. For the data obtained at FRC, the mean and range of these differences (centimeters of H_2O per liter per second) are as follows: normals, 0.12 (0.00–0.30); smokers, 0.22 (0.00–0.72); COPD, 0.48 (0.18–0.80). Frequency and magnitude differences, similar to the above, were also observed in the data obtained continuously and during inspiration.

For one subject (R. C.) with COPD, the respiratory impedance before and after inhalation of isoproterenol is shown (Fig. 9) both in polar coordinates ($|Z_{rs}|$ and θ_{rs}) and in rectangular coordinates as the real or resistive (R_{rs}) and imaginary or reactive (X_{rs}) parts of Z_{rs}.

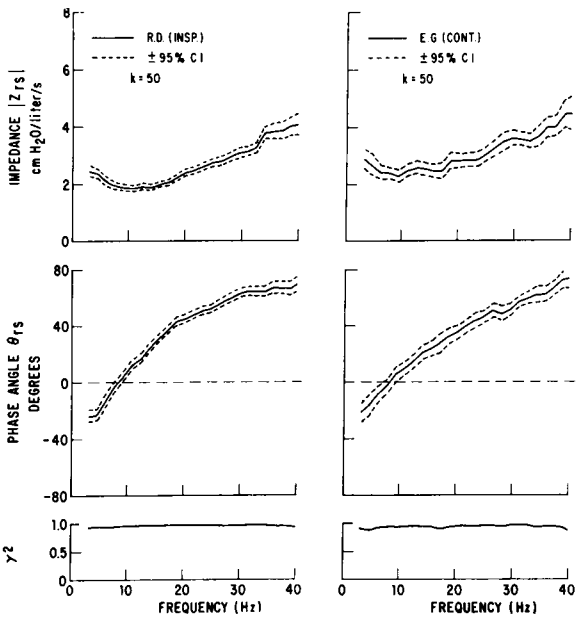

FIGURE 6 Magnitude and phase angle of Z_{rs} along with the coherence function (γ^2) and the calculated (Eqs. 13 and 14)±95% confidence intervals (CI). For subject E. G., measurement was obtained during continuous respiration and for subject R. D., during the inspiratory part of the respiratory cycle.

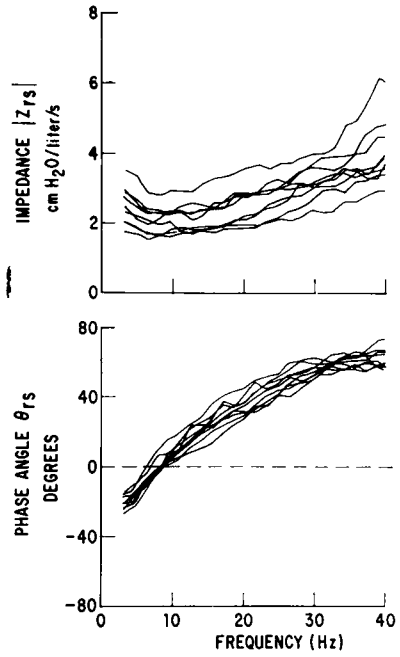

FIGURE 7 $|Z_{rs}|$ and θ_{rs} measured continuously during quiet breathing in nine normal subjects.

Fig. 10 shows $|Z_{rs}|$ and θ_{rs} obtained in a normal subject (E. M.), during slow panting (1–1.5 Hz) at FRC and at different volumes from 2.0 liters below to 2.5 liters above FRC. Z_{rs} is also displayed in rectangular coordinates as R_{rs} and X_{rs}.

DISCUSSION

General comments and variability of spectral estimates. The magnitude and phase angle of the repiratory impedance in the normal subjects (Figs. 4, 6, 7, 10) appear to be determined by approximately second-order characteristics. However, the curves are not as smooth as might be expected in a simple, linear, second-order, resistance-inertance-compliance (RIC) system. These observations can be explained, in part, both by physiological and statistical considerations. It has been emphasized by Shephard (6) that local resonances in branches of a complex series-parallel circuit may produce dips and peaks in the overall impedance curve. A difference in the frequency at which the impedance magnitude is minimum and at which the phase angle is zero, is consistant with circuits containing parallel elements, and is in keeping with various electrical models of the respiratory system (2, 6–8, 11–13), and the observations of DuBois et al. (3).

The behavior of complex circuits, such as the lung-chest system, may not be adequately described by a single, linear differential equation. Nonlinearities could introduce statistical variability into the spectral estimates which would be reflected by reduced values for coherence. A similar effect could be seen if any parameter in the system were changing nonlinearly with respect

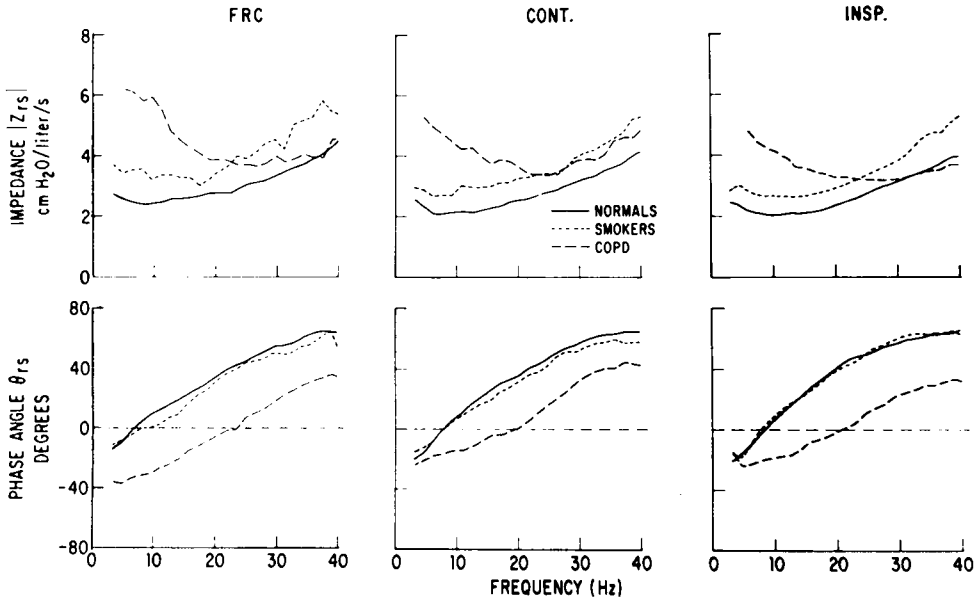

FIGURE 8 Mean $|Z_{rs}|$ or θ_{rs} for the three groups of subjects, measured continuously during quiet breathing (cont.), and during the inspiratory (insp.) and FRC portions of the respiratory cycle.

TABLE III

Impedance Magnitude ($|Z_{rs}|$), Phase (θ_{rs}), and Resonant Frequency (f_n)*

Group	Subject	f_n			$\|Z_{rs}\|$ at f_n			θ_{rs} at 12 Hz			$\|Z_{rs}\|$ at 40 Hz			θ_{rs} at 40 Hz		
		FRC	Cont.	Insp.	FRC	Cont.	Insp.	FRC	Cont.	Insp.	FRC	Cont.	Insp.	FRC	Cont.	Insp.
		Hz			*cm H_2O/liter/s*			*degrees*			*cm H_2O/liter/s*			*degrees*		
Normal	H. E.	5.9	6.9	6.7	1.85	2.00	2.13	+26.0	+19.5	+17.5	4.40	3.80	4.10	+66.0	+66.0	+66.0
	J. R.	8.0	8.5	9.5	2.68	2.83	3.00	+9.0	+7.0	+5.5	3.81	6.00	5.00	+58.0	+60.0	+54.0
	D. H.	7.0	8.9	9.1	2.13	1.62	1.63	+12.0	+13.0	+10.0	4.18	3.41	3.00	+53.0	+58.0	+63.0
	E. G.	6.4	8.3	9.0	1.82	2.36	1.92	+22.0	+13.0	+14.4	4.60	4.45	3.98	+74.0	+85.0	+83.0
	D. E.	6.7	6.1	7.7	1.66	1.58	1.69	+22.0	+23.5	+20.5	3.80	3.80	3.80	+64.0	+67.0	+62.0
	S. S.	6.2	8.6	8.1	3.16	2.28	2.10	+20.0	+20.0	+20.0	5.40	4.85	4.60	+46.0	+54.0	+54.0
	R. O.	5.6	7.8	8.6	2.48	1.70	1.90	+18.0	+19.0	+14.5	5.75	3.92	3.90	+73.0	+73.0	+73.0
	R. D.	6.8	8.3	8.0	3.18	2.32	1.94	+12.0	+13.0	+16.4	5.80	3.90	4.10	+61.0	+57.0	+70.0
	T. G.	8.5	9.0	8.7	3.10	2.06	2.30	+5.0	+9.0	+10.0	4.00	3.00	3.75	+57.0	+64.0	+65.0
	E. M.	‡	8.5	‡	‡	2.30	‡	‡	+8.1	‡	‡	3.91	‡	‡	+63.0	‡
	Mean§	6.79	8.04	8.38	2.45	2.08	2.07	+16.2	+15.2	+14.3	4.63	4.12	4.03	+61.3	+64.9	+65.6
	SD	0.95	0.96	0.85	0.61	0.41	0.41	7.0	5.5	5.0	0.81	0.88	0.56	9.1	9.5	9.1
	SE	0.32	0.32	0.28	0.20	0.14	0.14	2.3	1.8	1.7	0.27	0.30	0.19	3.0	3.2	3.0
Smokers	A. M.	14.4	8.0	8.3	5.60	2.61	1.79	−4.0	+10.5	+18.6	7.80	5.70	3.80	+63.0	+61.0	+73.0
	T. C.	5.4	5.9	6.5	3.15	3.19	5.18	+21.8	+21.0	+20.4	6.40	8.00	9.40	+56.0	+59.0	+63.0
	J. J.	15.9	8.2	9.6	1.95	2.80	1.39	−13.0	+11.0	+15.9	2.75	4.80	3.60	+50.0	+57.0	+70.0
	S. H.	6.9	8.5	7.6	2.60	2.26	2.21	+18.0	+12.0	+16.0	7.40	4.25	4.45	+62.0	+60.0	+60.0
	J. N.	7.4	9.2	9.9	2.41	2.38	2.60	+11.2	+5.5	+2.5	3.80	3.43	3.43	+55.0	+47.0	+44.0
COPD	W. S.	‡	21.3	‡	‡	5.21	‡	‡	−8.0	‡	‡	7.30	‡	‡	+32.0	‡
	G. L.	28.5	21.6	30.3	4.05	3.20	3.39	−24.0	−18.5	−31.0	3.59	4.07	3.90	+22.0	+26.0	+8.0
	F. H.	16.2	8.9	14.5	‡	3.50	2.60	−22.0	−7.0	−4.0	‡	6.55	4.12	+32.0	+59.0	+52.0
	R. B.	15.0	18.0	16.3	4.10	4.60	3.65	−4.2	−11.5	−7.5	5.30	5.60	4.30	+35.0	+31.0	+31.0
	R. C.	24.8	25.8	24.5	3.90	3.00	2.90	−43.0	−25.0	−21.0	5.00	3.65	2.92	+38.0	+39.0	+34.0

* Data from different portions of the respiratory cycle, abstracted from computer drawn curves similar to those shown in Figs. 4, 6–8. Measurements were made (see Methods) continuously during quiet breathing (Cont.), during inspiration (Insp.) and at FRC.

‡ Data not obtained (subjects E. M. and W. S.) or lost (subject F. H.).

§ Mean does not include Cont. values for subject E. M.

to time or the frequency of the random input; for example, variability in upper airway resistance or chest wall compliance during the respiratory cycle. Another factor which could result in variability of spectral estimates is the contamination of the output, of the system in question, by an extraneous "noise" source that is uncorrelated with the random input. The cardiogenic oscillations were found to be a source of uncorrelated noise in the flow signal but their effects on the spectral estimates of respiratory impedance were minimized by increasing the amplitude of the forced oscillations.

Characteristics of the mouth. The few available measurements of the mechanical properties of the mouth, either are unpublished or do not specify if the characteristics of the mouthpiece assembly were taken into account. Clements et al. (40) studied two normal subjects (checks relaxed), with the interrupter technique, by conducting air into one nostril at 0.5 or 1.0 liter/s and measuring mouth pressure, with the other nostril and glottis closed. From this they calculated that the resistance (R_M) and compliance (C_M) were 5 cm H_2O/liter per s and 0.001 liters/cm H_2O, respectively. From the frequency of oscillation after closure of the interrupter, they concluded that inertance (I_M) was negligible. Shephard (41) reports, from unpublished data, a range of 0.0004–0.0048 liters/cm H_2O for C_M. Mead[6] has measured C_M in one subject and found it to be 0.0008 liters/cm H_2O with the cheeks relaxed and 0.0004 liters/cm H_2O if the cheeks were supported. The random noise method provides the opportunity to obtain Z_M over a wide range of frequencies (Fig. 5, Table II).

Analysis of respiratory impedance in normal subjects. Fig. 11 shows the extent to which the mean impedance of the normal subjects can be described by a second-order system. The coefficients for the model of Z_{rs} were derived from the mean normal Z_{rs} (average of data in Fig. 7, see also Table III), assuming that, at 40 Hz, the measured net reactance ($X_{rs} = |Z_{rs}| \sin \theta_{rs}$) was essentially equal to inertial reactance and that compliant reactance was negligible. Respiratory inertance (I_{rs}) was estimated as $I_{rs} = X_{rs}/\omega$, where $\omega = 2\pi f$ and $f = 40$ Hz. C_{rs} was then computed assuming second-order RIC behavior, as $C_{rs} = (4\pi^2 f_n^2 I_{rs})^{-1}$ where f_n is the resonant frequency. The error in the estimation of I_{rs} in this way would be less than 3% for reasonable physiological values of $C_{rs} \cdot R_{rs}$ for the model was obtained simply as $|Z_{rs}|$ at $\theta_{rs} = 0$. The mean values,

[6] Dr. Jere Mead. Personal communication.

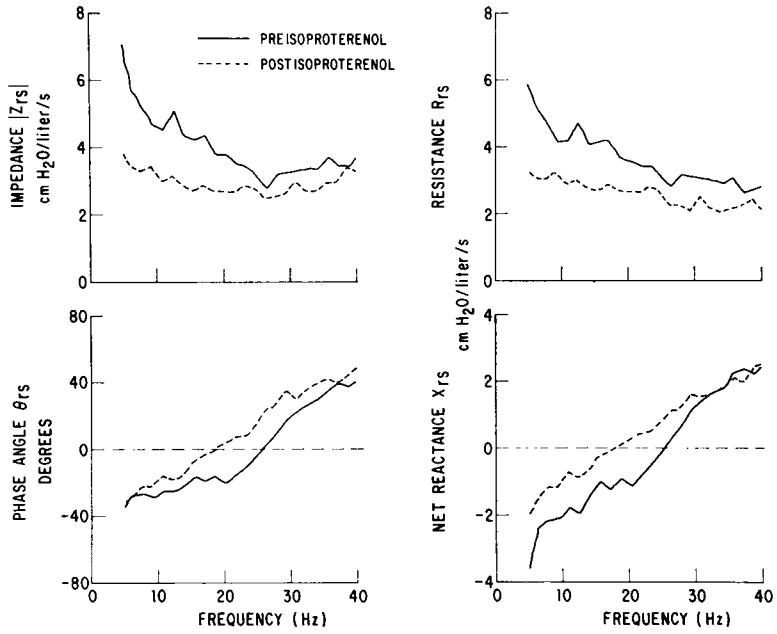

FIGURE 9 Components of the respiratory impedance obtained during quiet breathing in subject R. C. (COPD) before and after inhalation of isoproterenol. Z_{rs} is displayed in polar (left panels) and rectangular (right panels) coordinates.

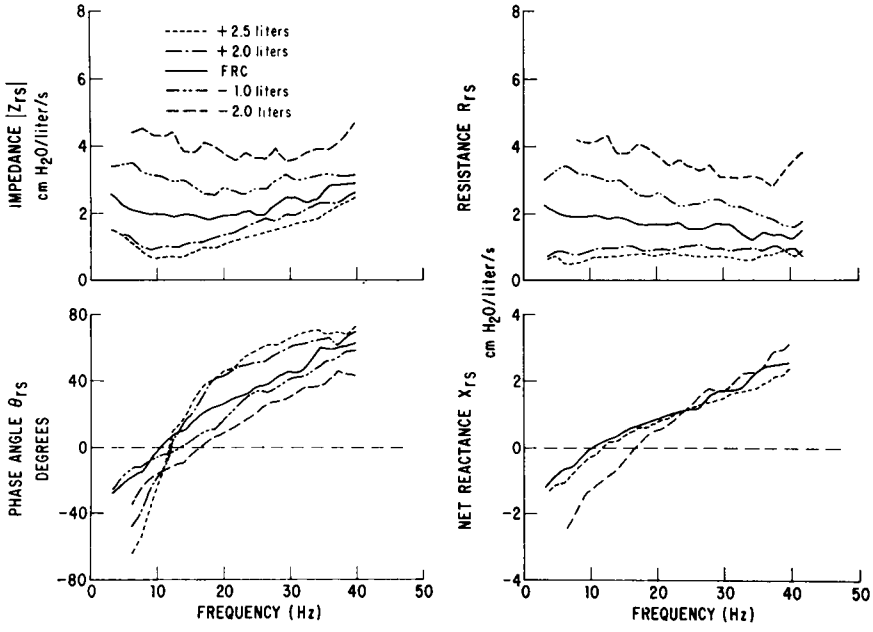

FIGURE 10 Polar (left) and rectangular (right) displays of Z_{rs} at different lung volumes in a normal subject (E. M.). The data obtained at 2.0 liters above and 1.0 liters below FRC have been omitted from the lower right-hand panel for clarity, since the curves were almost superimposed on those obtained at FRC and +2.5 liters.

range, and SD, for I_{rs} and C_{rs} estimated in this way for nine normal subjects are given in Table IV.

The respiratory impedance (Z_{rs}'), uncorrected for the effects of the mouth and mouthpiece assembly (Z_M'), is also modeled in Fig. 11. Z_M' is assumed to be an RC system in parallel with Z_{rs}. The R and C values for Z_M' were obtained from the average measured Z_M' (Fig. 3). The relationship between Z_{rs}, Z_{rs}', and Z_M' in the model is given by Eq. 15 and comparison with the mean data (Fig. 11) illustrates that Z_{rs} deviates only slightly from second-order behavior, primarily at frequencies less than 6 and greater than 25 Hz. The model also shows that correction of respiratory impedance assuming that Z_M' is a parallel RC pathway, is reasonable.

The values for $R_{rs}(|Z_{rs}|$ at $\theta_{rs} = 0)$, obtained by the spectral analysis technique in normal subjects (Table III), are similar to previously reported values for resistance measured by the forced oscillation technique (9, 24, 42). For the measurements made at FRC, the frequency at which $\theta_{rs} = 0$ (Table III) is in the range of 5.6–8.5 Hz, shown by some investigators (3, 9) to be the f_n of the respiratory system, but somewhat higher than reported by others (13, 20, 25). This could be due to differences in method or among subjects. Few measurements of the phase angle between pressure and flow, during forced oscillations, have been made at small frequency intervals over a wide range of frequencies. Most studies (3, 9, 18, 20) have been confined to observation of the phase relationship on an oscilloscope screen, and report, in some subjects, a single value for "in phase" resonance. Actually, several authors (3, 9, 21) have not been able to demonstrate a phase angle of 0 in some normal subjects, over a frequency range of 3–10 Hz. This could be explained by resonance occurring outside the frequency range studied—perhaps due to failure to take into account the parallel impedance of the mouth.

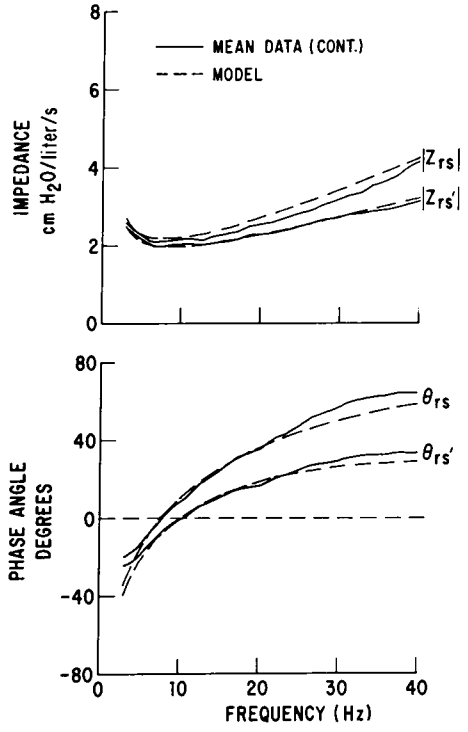

FIGURE 11 Components of total respiratory impedance with (Z_{rs}) and without (Z_{rs}') correction for the impedance of the mouth and mouthpiece assembly (Z_M'). The solid curves represent the mean values for the normal subjects (Fig. 7). The broken curves represent the impedance of a series circuit with coefficients derived from the mean data as described in the text. The relationships between Z_{rs}, Z_{rs}', and Z_M' are given by Eq. 15.

TABLE IV
*Respiratory Inertance (I_{rs}) and Compliance (C_{rs}) in Normal Subjects**

	I_{rs}‡			C_{rs}§		
	FRC	Cont.	Insp.	FRC	Cont.	Insp.
	cm H₂O/liter/s²			*liters/cm H₂O*		
Mean	0.0150	0.0146	0.0143	0.0361	0.0293	0.0262
Min	0.0129	0.0107	0.0106	0.0263	0.0170	0.0174
Max	0.0219	0.0207	0.0161	0.0455	0.0489	0.0378
SD	0.0025	0.0028	0.0017	0.0068	0.0102	0.0062

* Mean values, range, and SD of I_{rs} and C_{rs} derived from Z_{rs}, measured in nine normal subjects (Table II) continuously (Cont.), at FRC, or during inspiration (Insp.).
‡ I_{rs} estimated from net reactance (X_{rs}) at 40 Hz as described in the text.
§ C_{rs} computed as described in text, from individual values of I_{rs} and f_n (Table II).

Comparison to data of Peslin et al. (13). Fig. 12 shows the mean $|Z_{rs}|$ and θ_{rs} measured, during quiet breathing and at FRC, in the normal subjects by the random noise technique, compared to the average data of Peslin et al. (13). Using a body plethysmograph with an airtight neck seal, they measured total respiratory impedance at FRC in five normal subjects over a frequency range of 3–70 Hz by comparing, for magnitude and phase, sinusoidal perithoracic pressure oscillations with flow measured at the mouth. The f_n measured at FRC is similar in both studies. However, $|Z_{rs}|$ measured by Peslin et al. is higher and θ_{rs} is more positive at frequencies above f_n, compared to the random noise data, suggesting that the behavior of the respiratory system is determined by fourth-order characteristics. Factors which could possibly account for the differences between our data and those of Peslin et al. (13) will now be considered. Both real and theoretical differences in respiratory impedance, depending

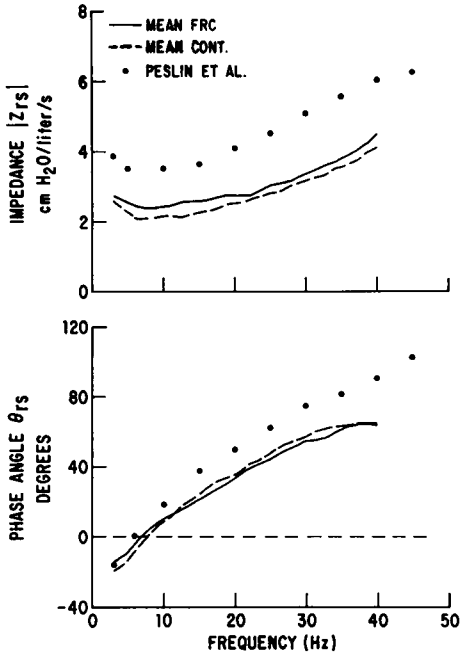

FIGURE 12 Comparison of mean normal data, measured continuously or at FRC during quiet breathing, to average data from five subjects studied by Peslin et al. (13).

on the site of application of the forced oscillations have been discussed by others (3, 6, 25). It can be shown that the impedance of a system, obtained when the input and the output (i.e., pressure and flow) are measured at the same point, is not necessarily the same as when the input is measured at one point and the output at a different point in the system. If the forced oscillations are applied at the mouth and both pressure and flow are measured at the mouth, the input impedance of the system is determined. On the other hand, if the oscillations are applied and pressure is measured around the chest and the resulting flow measured at the mouth, the so-called transfer impedance of the system is obtained. This impedance will be the same as the input impedance only if no parallel impedance is interposed between the sites of pressure and flow measurement. Thus, if the oscillations are applied around the chest, the flow measured at the mouth will be less than the total flow into the system depending on the distribution of and the extent to which compliance of gas or airways behave as a parallel elastic shunt. This could explain the larger impedance magnitude and more positive phase angle reported by Peslin et al. (13) compared to the present study (Fig. 12). The use of a neck seal could also contribute to the higher $|Z_{rs}|$ measured by Peslin et al.

Analysis of impedance in obstructed subjects. Although the individual variability of $|Z_{rs}|$ and θ_{rs} is greater among the obstructed subjects, as compared with the normal ones (Table III), several general conclusions may be drawn from observation of the mean data (Fig. 8). Regardless of the portion of the respiratory cycle sampled, the characteristics of normal subjects and the smokers approximate those of a second-order system, although the mean value of the minimum $|Z_{rs}|$ in the smokers is slightly greater. $|Z_{rs}|$ in the subjects with COPD is quite high at low frequencies and decreases to a minimum at a much higher frequency compared to the normals and smokers.

In both the normal and obstructed subjects θ_{rs} is negative at low frequencies. As frequency is increased, θ_{rs} in the normals and smokers crosses 0 and is in the range of 40° at 20 Hz and 60° at 40 Hz, although between 8 and 15 Hz θ_{rs}, measured at FRC, is less positive in the smokers. In the subjects with COPD, θ_{rs} does not cross 0 until approximately 20 Hz and remains less positive than in the normals and smokers. Since both resistance and inertance are inversely proportional to the radius of a tube, it might be expected that the obstructed subjects would have a higher inertance (and possibly a higher lung compliance) and hence a lower f_n when, in fact, the opposite appears to be the case. Thus, other factors must account for the observed differences between normal and obstructed subjects.

Consideration of data in terms of models of frequency-dependent mechanics. Otis et al. (2) using a two-compartment, parallel pathway analog of the lung, predicted that patients with obstructive lung disease should exhibit a fall in both compliance and resistance with increasing frequency due to an unequal distribution of time constants throughout the lung. Frequency dependence of compliance has been observed in patients with COPD (43) and has been used to determine the presence of early peripheral airways obstruction when the elastic properties of the lung are normal and airways resistance is still in the normal range (44, 45). Grimby et al. (10) and Hyatt et al. (24), using modifications of the forced oscillation technique demonstrated, in obstructed subjects, a fall in respiratory resistance with increasing frequency. This decrease in resistance can account in part for the decrease in impedance observed in our COPD subjects as frequency increases. The negative phase angle from 3 to 20 Hz and the high f_n in our subjects with COPD might be explained by a fall in compliance with frequency, keeping compliant reactance greater than inertial reactance. The negative phase angles we observed are consistent with the observations of others who have used the forced oscillation technique to study patients with obstructive lung disease. Grimby et al. (10) noted that often resonance could not be demonstrated at frequencies up to 10 Hz in patients with COPD. They suggested that reductions in dynamic compliance with increasing frequency, in

these patients, caused the f_n to remain above the applied frequency. Fisher et al. (9) showed that the phase angle between pressure and flow, in many subjects with emphysema, was not 0 at any frequency in the range of 2–10 Hz. These authors commented that the failure to detect resonance could be due to a change in effective compliance with frequency, keeping capacitive reactance greater than inductive reactance at all frequencies, and suggested that resonance might be found outside the frequency range studied. Sobel (21) was unable to find an f_n between 3 and 10 Hz in many normal subjects; and in all subjects with obstructive lung disease and he suggested that the airways, as a compliant element in parallel with the lung and chest, could account for phase shifts in lungs with increased resistance. Also, preliminary reports by others using electrical models (46) or high-frequency forced oscillations (47) have suggested that negative phase angles over a wide range of frequencies would be expected in patients with obstructive lung disease.

Three models of frequency dependence. Several two-compartment, parallel RC models have been proposed to explain the frequency dependence of compliance and resistance observed in obstructive lung disease. In the model of Otis et al. (2) time constants are unevenly distributed throughout the lung parenchyma. Another model, proposed by Hogg et al. (48) considers the resistance of channels for collateral ventilation to be too high to result in frequency-dependent behavior in normal lungs. But flow through these channels can become important with obstruction of the peripheral airways, causing time-constant discrepancies, between collaterally and normally ventilated areas of lung, accounting for frequency-dependent compliance in emphysematous lungs. Mead (11) considered the airways to be expanding structures in parallel with the air spaces, and using a two-compartment parallel model, showed that time-constant differences between the airways and the parenchyma caused frequency dependence of compliance and resistance. The fall in resistance and compliance predicted for normal subjects by Mead's model is too small to be apparent in measurements made at practical breathing frequencies, although there have been several reports of frequency-dependent compliance occurring in normal subjects (49–51). As peripheral airway resistance is increased, the time-constant differences between the airways and parenchyma become more prominent, and can account for most of the frequency-dependent behavior observed in diseased lungs without having to invoke a generalized distribution of peripheral time-constant discrepancies.

Analysis of data in terms of an electrical model of the total respiratory impedance. To determine to what extent frequency-dependent changes in the mechanical properties of the lung can account for our observations we have employed an electrical model of the respiratory system. The three different anatomical models described in the previous section, have all been interpreted within the framework of a single electrical analog model shown in Fig. 15 (Appendix). The two-compartment parallel section of the model (Z_{pp} in Fig. 15) has a different anatomical counterpart in each of the three models. Since all three of these anatomical models can be represented by a single electrical analog, each might explain the results, if the anatomical counterparts of the components in the electrical analogy are given appropriate characteristics. The conclusion, that any particular model is superior to another in terms of explaining the impedance data, may be drawn since the physical characteristics which must be applied to the rejected models are ridiculously unlikely.

The effective values for resistance and net reactance, arising from time-constant discrepancies in a parallel, two-compartment RIC pathway (Z_{pp} in Fig. 15), were incorporated in series with a circuit containing resistive, capacitive, and inductive components, representing respectively the lumped tissue, large and upper airway resistance, the chest wall resistance and compliance, and the total respiratory inertance, all three of which are shared by the parallel two-compartment portion of the model. It is then possible to determine the effect of parallel time-constant discrepancies on $|Z_{rs}|$ and θ_{rs} in the context of the mechanical properties shared by the two compartments. The equations describing the behavior of the model are shown in the Appendix.

Since X_{rs} is determined both by compliance and inertance, and our measurements of Z_{rs} were made at relatively high frequencies, the inertial component of the impedance cannot be neglected in the model. There is evidence (52–54) that the effect of inertance on the measurement of dynamic lung compliance is important at low frequencies. The assumption that inertance in an RIC system is negligible, implies that compliant reactance ($X_C = -1/\omega C$, $\omega = 2\pi f$) equals net reactance (X_T) when, actually, $X_T = X_I - X_C$, ($X_I = \omega I$). To the extent that X_C does not equal X_T, the dynamic compliance will increase with frequency. For reasonable values of lung or total inertance (0.010–0.015 cm H_2O/liter per s^2) dynamic compliance will begin to increase between 1 and 2 Hz and tend toward infinity as the f_n of the system is approached, above which the values for dynamic compliance would become negative. The effect of neglecting inertance on dynamic compliance would be greater for the lung alone than for the total respiratory system, which has a lower compliance due to the series chest wall component. Although the frequency-dependent properties in our model have been expressed in terms of total reactance (X_{rs}) and resistance (R_{rs}), it is still reasonable to think in terms of an effective value of compliance or inertance at a

given frequency if it is remembered that their effects cannot be separated by measurement.

Since inertance varies as the square and resistance as the fourth power of the radius, peripheral airway inertance must be a very small fraction of total inertance. The equations of Otis et al. (2), have been modified (Appendix) to include inertance terms. Uneven distribution of peripheral inertance had no effect on the total impedance (Z_{rs}) of the model because peripheral, compared to total, inertance is so small. Thus, peripheral inertance has been neglected and the frequency-dependent portion of the model may be considered in terms of the more familiar parallel RC network (2). The shared inertance however, greatly influences the effective reactance of the model.

The graphical solutions to Eqs. 1A-11A (Appendix), showing the effects of frequency on Z_{rs} that would be expected for time-constant discrepancies between the dead space (compliant airways) and parenchyma (11), produced by varying the peripheral airway resistance (models A-C) and compliance as in COPD (model D), are shown in Fig. 13. The values of compliance and resistance in the two parallel compartments are similar to those used by Mead (11). The curves shown in Fig. 13 are similar to those observed in our subjects (Figs. 8–10), suggesting that observation of f_n or of θ_{rs} in the range of 10–20 Hz provides an estimate of time-constant unevenness. The frequency dependence of effective compliance, which keeps compliant reactance greater than inertial as frequency is increased, results in negative values of net reactance. Hence θ_{rs} remains negative to higher frequencies as small airway obstruction increases.

Since it is not practical to show the graphical solutions for all of the models discussed, the coefficients used in these solutions, along with the resulting f_n, θ_{rs} at 12 Hz and the effects on peripheral and total resistance, are listed in Table V of the Appendix. It is important to realize that these coefficients (Table V), representing different discrete anatomical models, are used in a single electrical analogy (Fig. 15) where an infinite number of solutions are possible but which will explain the data only when R_2 is made to approach 0 and C_2 made very low. It will be seen that R_2 and C_2 refer to relatively normal lung in the models of Otis et al. (2) and Hogg et al. (48). Values R_2 and C_2 on the other hand, required to explain the data, seem ridiculously low for application to the normal lung, but quite appropriate for the centrally located airways in Mead's (11) model.

In the models of Otis et al. (2) and Hogg et al. (48), the fall in effective compliance is complete at 2–3 Hz and tends to approach some value of parenchymal com-

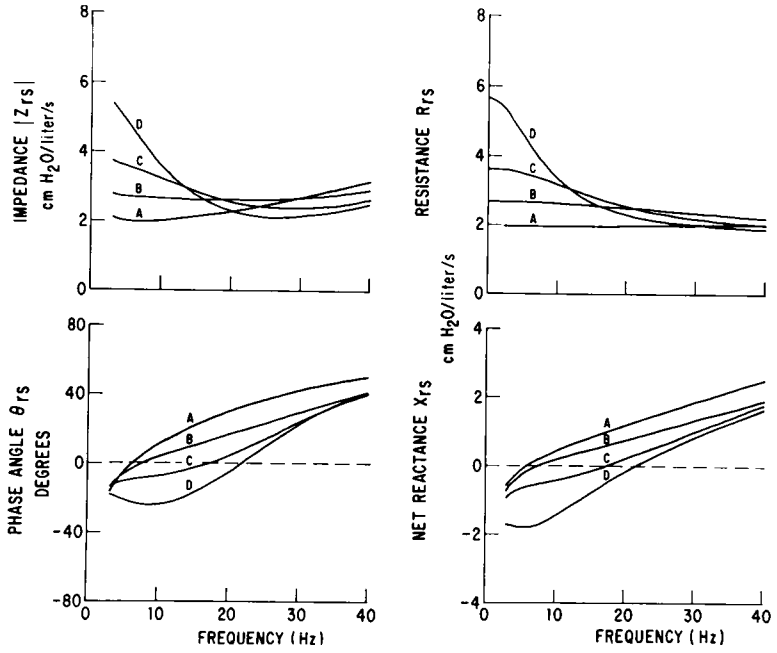

FIGURE 13 Polar (left) and rectangular (right) presentations of the solutions to Eqs. 1A–11A. Model A represents the normal respiratory system. Models B–D show the effect of increasing peripheral resistance and time-constant discrepancies between the airways and parenchyma (11). Lung compliance is increased (as might be expected in COPD) in model D. Note the similarities of this family of curves to the data (Figs. 8–10). The coefficients used in these and other models are given in Table V in the Appendix.

TABLE V

Characteristics of Various Lung Models

Model	Type*	R_1‡	R_2	C_1	C_2	V_1§	V_2§	T_1	T_2	f_n	θ_{rs} at 12 Hz	R_{pp}¶	R_{rs}
		cm H_2O/liter/s		*liters/cm H_2O*				*s*		*Hz*	*degrees*	*cm H_2O/liter/s*	
A	D	0.25	0.00	0.200	0.005	‖	‖	0.05	0.00	6.0	+15.9	0.24	1.99
B	D	1.00	0.00	0.200	0.005	‖	‖	0.20	0.00	8.0	+6.4	0.95	2.70
C	D	2.00	0.00	0.200	0.005	‖	‖	0.40	0.00	17.5	−6.2	1.90	3.65
D	D	4.00	0.00	0.400	0.005	‖	‖	1.60	0.00	22.0	−22.0	3.90	5.65
E	P	0.50	0.50	0.100	0.100	0.50	0.50	0.05	0.05	6.0	+16.5	0.25	2.00
F	P	2.00	0.50	0.100	0.100	0.50	0.50	0.20	0.05	6.3	+14.8	0.63	2.38
G	P	4.00	0.50	0.300	0.100	0.50	0.50	1.20	0.05	6.3	+15.7	2.28	4.03
H	P	0.36	0.83	0.140	0.060	0.70	0.30	0.05	0.05	6.0	+16.5	0.25	2.00
I	P	2.86	0.83	0.140	0.060	0.70	0.30	0.40	0.05	7.0	+12.8	1.47	3.22
J	P	2.86	0.83	0.340	0.060	0.70	0.30	0.97	0.05	7.0	+12.8	2.08	3.83
K	P	0.28	2.50	0.180	0.020	0.90	0.10	0.05	0.05	6.0	+16.5	0.25	2.00
L	P	2.22	2.50	0.180	0.020	0.90	0.10	0.40	0.05	7.0	+10.2	1.83	3.57
M	P	1.01	25.0	0.198	0.002	0.99	0.01	0.20	0.05	6.0	+12.9	0.99	2.74
N	C	0.50	0.00	0.100	0.100	0.50	0.50	0.05	0.00	6.5	+14.5	0.13	2.13
O	C	5.00	0.00	0.100	0.100	0.50	0.50	0.50	0.00	7.0	+14.1	1.25	3.25
P	C	15.00	0.00	0.100	0.100	0.50	0.50	1.50	0.00	7.0	+14.1	3.75	5.75
Q	C	5.00	0.00	0.400	0.100	0.50	0.50	2.00	0.00	7.0	+14.1	3.20	5.20
R	C	0.50	0.00	0.140	0.060	0.70	0.30	0.07	0.00	7.0	+13.1	0.25	2.25
S	C	5.00	0.00	0.140	0.060	0.70	0.30	0.70	0.00	8.0	+12.3	2.45	4.45
T	C	5.00	0.00	0.180	0.020	0.90	0.10	0.90	0.00	12.0	+0.2	4.05	6.05
U	C	5.00	0.00	0.380	0.020	0.90	0.10	1.90	0.00	12.0	+0.2	4.51	6.51
V	C	5.00	0.00	0.198	0.002	0.99	0.01	0.99	0.00	31.0	−18.8	4.90	6.90

* Type of time-constant uneveness between the compartments of Z_{pp}. P, peripheral, as described by Otis et al. (2); C, collateral, as described by Hogg et al. (48); D, dead space vs. peripheral lung, as described by Mead (11). C_1 represents collaterally ventilated lung in type C and the parenchyma and peripheral airways in type D.

§ V_1 and V_2 are the fractional volumes of the two compartments in *pp*. For all of the models (except E, H, and K in which $T_1 = T_2$) V_2 is the fast and V_1 the slow compartment.

‡ All values of R are rounded off to the second decimal.

‖ Not applicable since it is assumed that $C_1 \neq C_2$ because of intrinsic differences in tissue elasticity.

¶ R_{pp} is computed as $(R_1C_1^2 + R_2C_2^2)/(C_1 + C_2)^2$ which is $\lim_{\omega \to 0}$ Eq. 2A.

pliance which, if anything, might be increased in obstructive disease. Table V shows that Z_{rs} in these models is not affected. In Mead's model (11), effective compliance continues to decrease over most of the frequency range, approaching the very low value of the airways.

Thus far, the volumes of the two parallel compartments in the models of Otis et al. (2) and Hogg et al. (48) have been considered equal. If the volume of the fast compartment (shorter time constant) is small, its compliance could be quite low. In the model of Otis et al. (2) for example, if total lung compliance is 0.2 liters/cm H_2O and the volumes of the slow and fast compartments (V_1 and V_2, respectively) are distributed such that $V_1: V_2 = 0.7:0.3$, then C_1 and C_2 would be 0.14 and 0.06 liters/cm H_2O, respectively. If initially the resistances are assigned to make $R_1C_1 = R_2C_2$ and then R_1 is increased to produce a 4- to 20-fold difference in time constants, most of the fall in effective lung compliance, to about half of the static value, occurs at 3 Hz but θ_{rs} and f_n are only minimally affected. Even if $V_1: V_2$ were distributed 0.9:0.1 or 0.99:0.01, with $C_2 = 0.02$ or 0.002 liters/cm H_2O, the change in f_n and θ_{rs} is small (Table V).

Similar to Mead's model (11), the value of R_2 (and hence the time constant) of the normally ventilated (fast) compartment in the collateral model (48) is effectively 0. If the compartmental volumes in the collateral model are equal, the fall in effective compliance is limited and θ_{rs} is only slightly affected, even if the resistance is as high as 15 cm H_2O/liter per s or the time constant as long as 2.0 s for the collaterally ventilated pathway (Table V). If the volume of the fast, compared to the collateral, compartment is small, the model is similar to Mead's (11) in that the compliance of the fast compartment can be quite low. However, for the collateral model to produce changes in effective compliance that result in increased f_n and negative

values for θ_{rs} at higher frequencies, requires that the distribution of V_1: V_2 (collateral: normal) be 0.90:0.10 or 0.99:0.01 and the increases in peripheral resistance are even greater than in Mead's model (Table V).

It is possible that gas compressibility might cause parallel elastic shunt effects similar to those due to compliant airways. We have considered this in our model (assuming a gas compliance of 0.0035 liters/cm H_2O) and concluded that gas compressibility has no significant effect on the input impedance of the model. Gas compliance depends on volume, the majority of which is contained in the alveoli. The small volume of gas in the conducting airways accounts for a negligible portion of the total gas compressibility and the parallel elastic shunt due to gas compliance is between the small airways and the pleura. On the other hand, none of the airway compliance is located in the alveoli and the parallel shunt is between the airways and the alveoli. We have modeled several distributions of airway compliance and our data can best be explained by a distribution localizing most of the airway compliance in the small airways.

Thus, although the frequency dependence of effective compliance in obstructive lung disease, over the range of practically achievable breathing frequencies, can be explained by any of the three parallel two-compartment models (and more than one of these models may be simultaneously contributing to the behavior of the lung), our measurements of $|Z_{rs}|$ and θ_{rs} can best be accounted for by time-constant discrepancies between the airways and the air spaces, as described by Mead (11).

Administration of a bronchodilator in a subject with COPD (Fig. 9) resulted in a fall of f_n from 25.8 to 18.6 Hz, a less negative X_{rs} over most of the frequency range (less frequency dependence of compliance), and R_{rs} was less frequency dependent. The similarity between Fig. 9 and the model (Fig. 13), is consistent with a fall in peripheral resistance after the bronchodilator.

Differences dependent on the phase of the respiratory cycle. Most previous measurements employing the forced oscillation technique have been made at FRC. There are differences in $|Z_{rs}|$ and θ_{rs} depending on the portion of the respiratory cycle sampled for analysis (Table III, Fig. 8). Although the data obtained continuously during quiet breathing represent a different time sample of the respiratory system and cannot be directly compared to that sampled during inspiration (between 0.25 and 0.5 liters/s) or at FRC, several conclusions may be drawn from the observed differences.

Using the forced oscillation technique, Peslin et al. (55) measured total respiratory resistance during the respiratory cycle in normal subjects. They found that the resistance followed variations in respiratory flow, although the degree of change in resistance for a given flow was variable between subjects. In the present study, $R_{rs}(|Z_{rs}|$ at $f_n)$ measured during early inspiration (corresponding approximately to inspiratory fraction 2 of Peslin et al. [55]), compared to FRC, was slightly higher (2–15%) in four and moderately lower (20–64%) in five of our normal subjects. This variability could be due to different respiratory flows at the time of measurement or variability of upper airway area.

f_n in the normal subjects was uniformly higher ($P < 0.001$) during inspiration compared to FRC (Table III). This can be explained in part by a fall in airway inertance during inspiration. The subjects exhibiting the largest falls in R_{rs} during inspiration also had greater increases in f_n. Since resistance depends both on the magnitude of respiratory flow and on cross-sectional area, it is not possible to estimate the change in I_{rs} from the observed change in R_{rs}. If R_{rs} was minimally dependent on flow, as in one of the subjects reported by Peslin et al. (55), I_{rs} estimated from the observed differences in R_{rs} at FRC and during inspiration (Table III) would not be sufficient to account for the observed increase in f_n. Thus, an inspiratory fall in R_{rs}, due to an increase in airway diameter, must be masked by a flow related increase in R_{rs}, or other factors (such as a fall in lung or chest wall compliance) may account for the higher f_n observed during inspiration.

In the obstructed patients (Table III, Fig. 8) additional factors such as dynamic compression of large airways during respiration, or small airway closure at FRC could partially account for the greater differences in Z_{rs} between different parts of the respiratory cycle. The latter might reduce lung compliance or produce a greater frequency dependence of effective compliance and an increase of f_n.

Effects of lung volume. The effects of lung volume on the components of the total respiratory impedance are shown in Fig. 10. As lung volume increases, R_{rs} falls and the system appears less damped. The family of $|Z_{rs}|$ and θ_{rs} curves is very similar to that of a second-order system with various degrees of damping (4). At 2.0 and 2.5 liters above FRC, f_n is slightly higher than at FRC, presumably due to lower inertance or increased stiffness of the system. Below FRC, where R_{rs} and I_{rs} are greater and f_n might be expected to fall, f_n increases. The increase of f_n at low lung volumes could be accounted for by a fall in effective compliance with frequency in part due to an increase of small airway resistance and increasing time-constant discrepancies between larger airways and alveoli as lung volume is reduced (i.e., by Mead's model as discussed earlier). The frequency dependence of R_{rs} at low lung volumes (Fig. 10) is also consistent with this explanation. A fall in chest wall compliance or a fall in lung compliance,

as the lung volume at which airway closure occurs is approached, might contribute to the increase of f_n at lower lung volumes.

Effects of the parallel shunt impedance of the mouth. The correction of the measured respiratory impedance for the parallel shunt impedance of the mouth (Eq. 15, Fig. 4) is greater as Z_{rs} is increased, since relatively more of the induced flow is shunted via the mouth. This means that $|Z_{rs}'|$ will underestimate differences, among subjects with varying degrees of airway obstruction, compared to $|Z_{rs}|$. On the other hand, if the observed phase angle (θ_{rs}') is not corrected for the mouth pathway, θ_{rs}' will be more negative than θ_{rs} at all frequencies. This is consistent with reports (3, 9, 21) that in some normal subjects resonance has not been detected. Also, the uncorrected $f_n(f_n')$ is higher for a given increase in R_{rs} and there is a greater difference in f_n' among subjects with varying degrees of obstruction. These relationships are illustrated in Fig. 14.

Further considerations of data in normal subjects. The deviation of Z_{rs}, in the normal subjects (Fig. 11), from second-order behavior is further illustrated by calculation of $R_{rs}(|Z_{rs}| \cos \theta_{rs})$, which shows that R_{rs} is frequency dependent, falling approximately 20% between 5 and 40 Hz. This fall in R_{rs} can account for the observation that the minimum value for $|Z_{rs}|$ occurs at frequencies slightly higher than f_n. Models B-D, L, N, and R-V (Table V) show differences between f_n and the frequency at which $|Z_{rs}|$ is minimum, similar to the observed (Results section) values.

The estimates of respiratory inertance (Table IV) show little variability and are in the range of previously reported measurements (3, 20, 52–53, 56–57). The calculated values of C_{rs}, on the other hand, are more variable and, assuming a static lung compliance of 0.2 liters/cm H_2O, would require that the average chest wall compliance (C_W) be about 0.031 liters/cm H_2O, somewhat lower than most previously reported static measurements (16, 50). A similar discrepancy was noted by DuBois et al. (3) who attributed it to the failure of the lungs and chest wall to behave as a single, lumped system. More specifically, perhaps, the variability and low value for C_{rs} could be due to a low C_W during continuous breathing, dependence of the calculated C_{rs} on both the f_n and estimated inertance, or a fall in effective lung compliance at the higher frequencies. The observed fall in R_{rs} suggests that the latter possibility is reasonable. The values of C_{rs} in Table IV are also consistent with previously reported changes of C_{rs} with frequency (50).

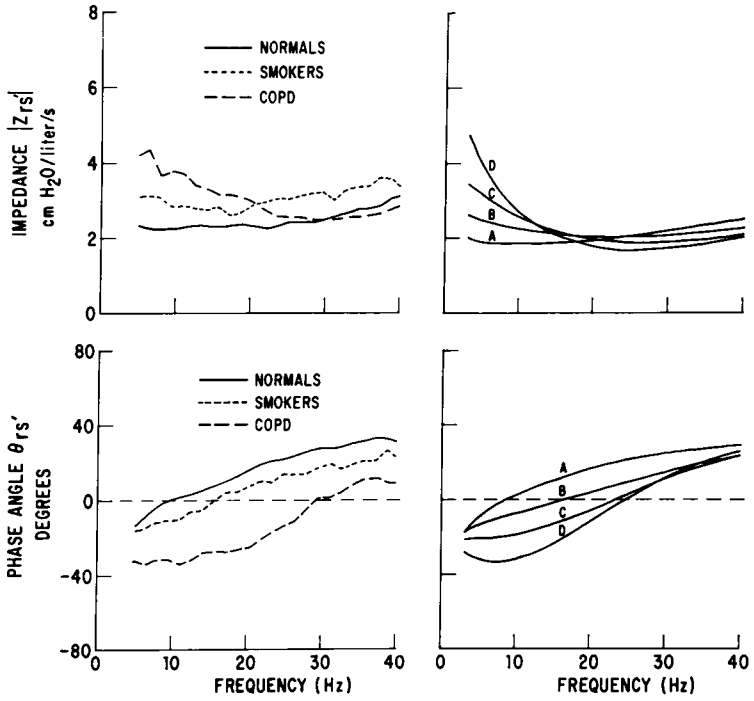

FIGURE 14 Components of the respiratory impedance, uncorrected for the parallel shunt impedance of the mouth. Left panels represent the mean data obtained during quiet breathing, in the three groups of subjects. Right panels show the graphical solutions to the same models illustrated in Fig. 13, except that the shunt impedance of the mouth (Fig. 5) is included.

It is of interest that, in several subjects, R_{rs} tended to increase between 30 and 45 Hz. At these higher frequencies, an uneven distribution of R/I time constants would be expected to result in an increase in effective resistance and inertance, similar to the fall in effective compliance and resistance described by Otis et al. (2), due to RC time-constant uneveness. This type of behavior may also account for some of the previously described characteristics of the mouth.

Some final comments. Although the random noise method may appear complicated at first, once the computer program and response characteristics of the instrumentation are worked out, the rapid measurement of the magnitude and phase of the respiratory impedance over a large range of frequencies by this method is relatively simple. In addition to improving our understanding of the dynamic mechanical properties of the respiratory system, interpretation of the data obtained in this study, in terms of an electrical model, suggests that frequency dependence of respiratory resistance or reactance, as well as the phase angle between pressure and flow at certain frequencies provides a "noninvasive" means of assessing the uneven distribution of lung time constants in disease.

APPENDIX

Fig. 15 shows an electrical analog of the respiratory system in which a two-compartment parallel pathway (pp) is incorporated into a model representing the components of the respiratory impedance shared by pp. By computing the impedance (Z_{pp}) of this pathway, it is possible to determine the effect of uneven time constants in pp on the total respiratory impedance. This allows interpretation of our data in terms of the apparent frequency dependence of mechanical properties which may arise from time-constant discrepancies in pp. By selection of appropriate coefficients, the two compartments of pp may represent two peripheral areas (2), collateral and normally ventilated lung (48), or the properties of the large airways and peripheral units (11). The impedance of pp is given by

$$Z_{pp} = R_{pp} + jX_{pp}, \tag{1A}$$

where R_{pp} is the real or resistive part, and X_{pp} the imaginary or reactive part of Z_{pp}. $j = \sqrt{-1}$.

The equations of Otis et al. (2) have been modified to include the effects of inertance in each compartment of pp:

$$R_{pp} = \frac{\omega^4(GD\text{-}BF) + \omega^2(AF - DH - EG) + (EH - CF)}{\omega^4G^2 + \omega^2(F^2 - 2GH) + H^2}, \tag{2A}$$

$$X_{pp} = \frac{\omega^6BG + \omega^4(FD - AG - BH) + \omega^2(AH + GC - FE) - HC}{\omega^5G^2 + \omega^3(F^2 - 2GH) + \omega H^2}, \tag{3A}$$

where

$$A = R_1R_2 + \frac{I_1}{C_2} + \frac{I_2}{C_1}, \quad B = I_1I_2, \quad C = \frac{1}{C_1C_2},$$

$$D = R_1I_2 + R_2I_1, \quad E = \frac{R_1}{C_2} + \frac{R_2}{C_1}, \quad F = R_1 + R_2,$$

$$G = I_1 + I_2, \quad H = \frac{1}{C_1} + \frac{1}{C_2}, \quad \text{and} \quad \omega = 2\pi f.$$

By incorporating the shared resistance (R_{uaw}) and inertance (I_{uaw}) of the large and upper airways (for simplicity, tissue inertance is neglected and all of the shared inertance is assumed to be airway), the pulmonary impedance (Z_L) may be computed as follows:

$$Z_L = R_L + jX_L, \tag{4A}$$

where

$$R_L = R_{pp} + R_{uaw}, \tag{5A}$$

and

$$X_L = X_{pp} + \omega I_{uaw}. \tag{6A}$$

The total respiratory impedance (Z_{rs}) may be obtained by including (C_W) the series chest wall compliance (for simplicity, small tissue and chest wall resistance are incorporated into R_{uaw}):

$$Z_{rs} = R_{rs} + jX_{rs} \tag{7A}$$

$$R_{rs} = R_L \tag{8A}$$

$$X_{rs} = X_L - \frac{1}{\omega C_W}. \tag{9A}$$

Z_{rs} may alternately be expressed in terms of magnitude ($|Z_{rs}|$) and phase angle (θ_{rs}):

$$|Z_{rs}| = \sqrt{R_{rs}^2 + X_{rs}^2}, \tag{10A}$$

$$\theta_{rs} = \tan^{-1}\frac{X_{rs}}{R_{rs}}. \tag{11A}$$

The measurement of respiratory impedance with forced oscillations applied at the mouth, includes the parallel shunt

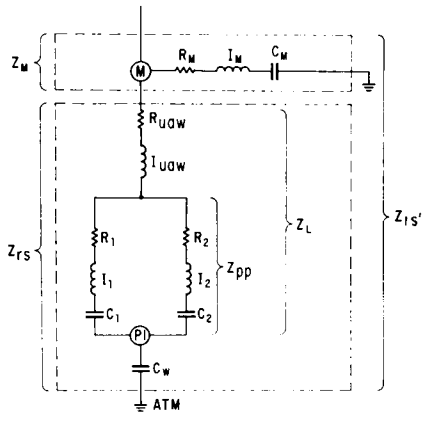

FIGURE 15 Electrical analog of respiratory system used in interpretation of data. The abbreviations are defined in the Appendix. ATM represents atmosphere (electrical ground); M, mouth; Pl, plural space.

impedance of the mouth (Z_M); the relationship of the measured respiratory impedance (Z_{rs}') to Z_{rs} and Z_M' is given by Eq. 15 in the Methods section. For the purposes of the electrical model:

$$Z_M = R_M + jX_M \tag{12A}$$

$$X_M = \omega I_M - \frac{1}{\omega C_M}. \tag{13A}$$

The coefficients R_M, C_M, and I_M may be derived from the mean Z_M data either including (Fig. 3) or excluding (Fig. 5) the characteristics of the mouthpiece assembly.

Using the above equations, it is possible to compute the magnitude and phase angle of the total respiratory impedance that would be expected for various combinations of R, I, and C in the model. Table V lists the coefficients used for models A-D (plotted in Fig. 13), as well as those used in several other models that are discussed but not plotted because of space availability. For the models listed in Table V, only R_1, R_2, C_1, and C_2 are varied to determine the effects on Z_{rs} of time-constant discrepancies in pp, produced by the various pathophysiologic situations described in the text. Also given in Table V are the fractional volumes and time constants of the two compartments; the expected f_n and θ_{rs} at 12 Hz; and the resulting peripheral (R_{pp}) and total (R_{rs}) respiratory resistance.

For the models listed in Table V, R_{uaw} = 1.75 (types P and D) or 2.0 (type C), and C_W = 0.1. I_{uaw} = 0.010–0.011, depending on the increase in peripheral inertance associated with the increase in R_{pp}. Actually this range of I_{uaw} had negligible effect on Z_{rs}. As mentioned in the Discussion section, the partitioning of inertance had no effect on Z_{rs} since I_1 and I_2 were so small relative to I_{uaw} and may be considered zero for the models listed in Table V.

ACKNOWLEDGMENTS

The authors are grateful to MSGT. A. J. Marchetti for technical assistance, Mr. R. A. Balusek and Mr. D. Threatt for their help in computer programming, Dr. H. M. Hughes for advice concerning statistical aspects of random noise, Mrs. E. Ferguson for repeated typing of the manuscript, and to Dr. Jere Mead for several helpful suggestions during the early portions of this study.

The voluntary informed consent of the subjects used in this research was obtained in accordance with Air Force Regulation 80-33.

REFERENCES

1. Olson, H. F. 1958. Dynamical Analogies. Van Nostrand Reinhold Co., New York, 2nd edition. 278 pp.
2. Otis, A. B., C. B. McKerrow, R. A. Bartlett, J. Mead, M. B. McIlroy, N. J. Selverstone, and E. P. Radford, Jr. 1956. Mechanical factors in distribution of pulmonary ventilation. *J. Appl. Physiol.* **8**: 427–443.
3. DuBois, A. B., A. W. Brody, D. H. Lewis, and B. F. Burgess, Jr. 1956. Oscillation mechanics of the lungs and chest in man. *J. Appl. Physiol.* **8**: 587–594.
4. Brody, A. W., A. B. DuBois, O. I. Nisell, and J. Engelberg. 1956. Natural frequency, damping factor and inertance of the chest-lung system in cats. *Am. J. Physiol.* **186**: 142–148.
5. Hull, W. E., and E. C. Long. 1961. Respiratory Impedance and volume flow at high frequency in dogs. *J. Appl. Physiol.* **16**: 439–443.
6. Shephard, R. J. 1966. Dynamic characteristics of the human airway and the behavior of unstable breathing systems. *Aerosp. Med.* **37**: 1014–1021.
7. Rowlands, G. F., K. R. Maslin, and L. H. Hutton. 1964. Frequency response of the human breathing system, to an input oscillating pressure-wave. Royal Aircraft Establishment Technical Memorandum ME. 291. Farnborough, Hants. 1–28.
8. Maslin, K. R., and G. F. Rowlands. 1966. A new method of measuring the impedance of the human respiratory system at moderate frequencies. Royal Aircraft Establishment Technical Report 66296. Farnborough, Hants. 1–41.
9. Fisher, A. B., A. B. DuBois, and R. W. Hyde. 1968. Evaluation of the forced oscillation technique for the determination of resistance to breathing. *J. Clin. Invest.* **47**: 2045–2057.
10. Grimby, G., T. Takishima, W. Graham, P. Macklem, and J. Mead. 1968. Frequency dependence of flow resistance in patients with obstructive lung disease. *J. Clin. Invest.* **47**: 1455–1465.
11. Mead, J. 1969. Contribution of compliance of airways to frequency-dependent behavior of lungs. *J. Appl. Physiol.* **26**: 670–673.
12. Van Den Berg, Jw. 1960. An electrical analogue of the trachea, lungs and tissues. *Acta Physiol. Pharmacol. Neerl.* **9**: 361–385.
13. Peslin, R., C. Duvivier, and J. M. Lambert. 1972. Réponse en fréquence du système mécanique ventilatoire total de 3 A 70 Hz. *Bull. Physio-Pathol. Respir.* **8**: 267–279.
14. Hilberman, M., R. W. Stacy, and R. M. Peters. 1972. A phase method of calculating respiratory mechanics using a digital computer. *J. Appl. Physiol.* **32**: 535–541.
15. 1972. Symposium on models in ventilatory mechanics. *Bull. Physio-Pathol. Respir.* **8**(no. 2): 181–432.
16. Mead, J., and J. Milic-Emili. 1964. Theory and methodology in respiratory mechanics with glossary of symbols. *Handb. Physiol.* **1** (Sect. 3): 363–376.
17. Cuenod, M., and A. P. Sage. 1968. Comparison of some methods used for process identification. *Automatica.* **4**: 235–269.
18. DuBois, A. B., and B. B. Ross. 1951. A new method for studying mechanics of breathing using cathode ray oscillograph. *Proc. Soc. Exp. Biol. Med.* **78**: 546–549.
19. Zechman, F. W., Jr., D. Peck, and E. Luce. 1965. Effect of vertical vibration on respiratory airflow and transpulmonary pressure. *J. Appl. Physiol.* **20**: 849–854.
20. Sharp, J. T., J. P. Henry, S. K. Sweany, W. R. Meadows, and R. J. Pietras. 1964. Total respiratory inertance and its gas and tissue components in normal and obese men. *J. Clin. Invest.* **43**: 503–509.
21. Sobol, B. J. 1968. Tests of ventilatory function not requiring maximal subject effort. II. The measurement of total respiratory impedance. *Am. Rev. Respir. Dis.* **97**: 868–879.
22. Grimby, G. 1969. Measurement of respiratory resistance with forced oscillations. *Scand. J. Clin. Lab. Invest. Suppl.* **110**: 37–39.
23. Goldman, M., R. J. Knudson, J. Mead, N. Peterson, J. R. Schwaber, and M. E. Wohl. 1970. A simplified measurement of respiratory resistance by forced oscillation. *J. Appl. Physiol.* **28**: 113–116.
24. Hyatt, R. E., I. R. Zimmerman, G. M. Peters, and W. J. Sullivan. 1970. Direct writeout of total respiratory resistance. *J. Appl. Physiol.* **28**: 675–678.
25. Atlan, G., P. Varene, Ch. Jacquemin, R. Pouliquen, J. F. Boisvieux, and J. Richalet. 1971. Étude critique

des méthodes d'oscillations forcées en méchanique Ventilatoire. *Bull. Physio-Pathol. Respir.* **7**: 63–78.
26. 1967. Special Issue on the fast Fourier transform. *IEEE Trans. Audio Electroacoustics.* **15**(no. 2): 44–113.
27. Cooley, J. W., and J. W. Tukey. 1965. An algorithm for the machine calculation of complex Fourier series. *Math. Comput.* **19**: 297–301.
28. Bergland, G. D. 1969. A guided tour of the fast Fourier transform. *IEEE Spectrum.* **6**: 41–52.
29. Blackman, R. B., and J. W. Tukey. 1958. The Measurement of Power Spectra. Dover Publications, Inc., New York. 190 pp.
30. Bendat, J. S., and A. G. Piersol. 1966. Measurement and Analysis of Random Data. John Wiley & Sons, Inc., New York. 390 pp.
31. Jenkins, G. M., and D. G. Watts. 1968. Spectral Analysis and Its Applications. Holden-Day, Inc., San Francisco. 525 pp.
32. Galloway, D. G., and B. F. Womack. 1969. An application of spectral analysis and digital filtering to the study of respiratory sinus arrhythmia. AFOSR 69-2048 TR, Electronics Research Center, University of Texas at Austin, Technical Report. no. 71. 172 pp.
33. Roth, P. R. 1971. Effective measurements using digital signal analysis. *IEEE Spectrum.* **8**: 62–70.
34. Richards, P. I. 1967. Computing reliable power spectra. *IEEE Spectrum.* **4**: 83–90.
35. Taylor, M. G. 1966. Use of random exitation and spectral analysis in the study of frequency-dependent parameters of the cardiovascular system. *Circ. Res.* **18**: 585–595.
36. Fry, D. L. 1960. Physiologic recording by modern instruments with particular reference to pressure recording. *Physiol. Rev.* **40**: 753–788.
37. Finucane, K. E., B. A. Egan, and S. V. Dawson. 1972. Linearity and frequency response of pneumotachographs. *J. Appl. Physiol.* **32**: 121–126.
38. Peslin, R., J. Morinet-Lambert, and C. Duvivier. 1972. Étude de la réponse en fréquence de pneumotachographes. *Bull. Physio-Pathol. Respir.* **8**: 1363–1376.
39. Comroe, J. H., Jr., S. Y. Botelho, and A. B. DuBois. 1959. Design of a body plethysmograph for studying cardiopulmonary physiology. *J. Appl. Physiol.* **14**: 439–444.
40. Clements, J. A., J. T. Sharp, R. P. Johnson, and J. O. Elam. 1959. Estimation of pulmonary resistance by repetitive interruption of airflow. *J. Clin. Invest.* **38**: 1262–1270.
41. Shephard, R. J. 1963. Mechanical characteristics of the human airway in relation to use of the interrupter valve. *Clin. Sci. (Oxf.).* **25**: 263–280.
42. Frank, N. R., J. Mead, and J. L. Whittenberger. 1971. Comparative sensitivity of four methods for measuring changes in respiratory flow resistance in man. *J. Appl. Physiol.* **31**: 934–938.
43. Mead, J., I. Lindgren, and E. A. Gaensler. 1955. The mechanical properties of the lungs in emphysema. *J. Clin. Invest.* **34**: 1005–1016.
44. Macklem, P. T., and J. Mead. 1967. Resistance of central and peripheral airways measured by a retrograde catheter. *J. Appl. Physiol.* **22**: 395–401.
45. Woolcock, A. J., N. J. Vincent, and P. T. Macklem. 1969. Frequency dependence of compliance as a test for obstruction in the small airways. *J. Clin. Invest.* **48**: 1097–1106.
46. Franck, J. B., L. E. Ostrander, and E. H. Chester. 1971. The frequency dependent behavior of pulmonary mechanics in obstructive lung disease. Proceeding of the 24th Annual Conference on Engineering in Medicine and Biology. 226 pp.
47. Kahn, A. R., and W. L. Childs. 1969. Measurement of mechanical properties of the pulmonary system—A new technique. The 8th International Conference on Medical Electronics and Biological Engineering. 21–8.
48. Hogg, J. C., P. T. Macklem, and W. M. Thurlbeck. 1969. The resistance of collateral channels in excised human lungs. *J. Clin. Invest.* **48**: 421–431.
49. Mills, R. J., G. Cumming, and P. Harris. 1963. Frequency-dependent compliance at different levels of inspiration in normal adults. *J. Appl. Physiol.* **18**: 1061–1064.
50. Albright, C. D., and S. Bondurant. 1965. Some effects of respiratory frequency on pulmonary mechanics. *J. Clin. Invest.* **44**: 1362–1370.
51. Ingram, R. H., Jr., and C. F. O'Cain. 1971. Frequency dependence of compliance in apparently healthy smokers vs. non-smokers. *Bull. Physio-Pathol. Respir.* **7**: 195–210.
52. Mead, J. 1956. Measurement of inertia of the lungs at increased ambient pressure. *J. Appl. Physiol.* **9**: 208–212.
53. Varene, P., and C. Jacquemin. 1970. La compliance effective. *Bull. Physio-Pathol. Respir.* **6**: 885–891.
54. Dosman, J., R. Antic, F. Bode, J. Urbanetti, R. Martin, and P. T. Macklem. 1973. Factors influencing dynamic lung compliance in man. *Physiologist.* **16**: 297. (Abstr.)
55. Peslin, R., T. Hixon, and J. Mead. 1971. Variations des résistances thoraco-pulmonaire au cours du cycle ventilatoire étudiées par méthod d'oscillation. *Bull. Physio-Pathol. Respir.* **7**: 173–186.
56. Bergman, N. A. 1970. Measurement of respiratory inertance in anesthetized subjects. *Respir. Physiol.* **9**: 65–73.
57. Jaeger, M. J., and A. B. Otis. 1964. Measurement of airway resistance with a volume displacement body plethysmograph. *J. Appl. Physiol.* **19**: 813–820.